Single-Core PAHs in Petroleum- and Coal-Derived Asphaltenes: Size and Distribution from Solid-State NMR Spectroscopy and Optical Absorption Measurements

R. Dutta Majumdar,[†,‡] K. D. Bake,[§] Y. Ratna, [†,‡] A. E. Pomerantz,[§] O.C. Mullins,[*§] M. Gerken,[†,‡] P. Hazendonk,[*†,‡]

[†]Department of Chemistry and Biochemistry, University of Lethbridge, Alberta T1K 3M4, Canada

[‡]Canadian Centre for Research in Advanced Fluorine Technologies, University of Lethbridge, Alberta T1K 3M4, Canada

[§]Schlumberger-Doll Research, Cambridge, Massachusetts 02139, United States

[*]Email: paul.hazendonk@uleth.ca, mullins1@slb.com

R. Dutta Majumdar's current address: Environmental NMR Centre, Dept. of Physical and Environmental Sciences, University of Toronto at Scarborough, 1265 Military Trail, Toronto, Canada M1C 1A4

Abstract

Solid-state ^{13}C NMR spectroscopy of two different asphaltenes, one derived from petroleum and the other from coal liquids, demonstrates that asphaltenes consist of a spectrum of large (>9) and small (<5) single-core polyaromatic hydrocarbon (PAH) molecules, with the larger PAHs dominating. It is shown that smaller PAHs are likely more abundant in the coal-derived asphaltenes, while the largest PAH cores of the two different asphaltenes are similar in size. These observations are reinforced by optical absorption. The coal-derived asphaltenes were found to contain a small fraction of archipelago-type structures, where a small PAH is tethered to the larger PAH core via an aryl linkage, which are less evident, and likely less abundant in the petroleum asphaltenes. An important difference between the two asphaltenes lies in their alkyl fraction, with the petroleum asphaltenes possessing significantly longer and more mobile alkyl sidechains, on average ~7 carbons long, as opposed to an average chain length of ~3-4 in the coal asphaltenes. The petroleum asphaltenes also possess a larger fraction of alicyclics. The longer length increases the propensity of the petroleum asphaltene alkyl sidechains to intercalate between the aromatic rings of adjacent asphaltene aggregates, which is not observed in coal-derived asphaltenes. This paper demonstrates the utility of combining cross-polarization based techniques and quantitative ^{13}C solid-state NMR spectroscopy in studying asphaltenes, while adding to the body of evidence supporting the single-core model of asphaltenes, which appears to be the dominant structural motif for this fraction of petroleum.

1. Introduction

The importance of understanding the molecular and colloidal structure of asphaltenes continues to increase. In the past, uncertainties regarding asphaltene structure have led to a phenomenological approach to asphaltene science in various applications, for example, the lack of ab initio approach to first-principles equation of state to treat asphaltene (thus viscosity) gradients in oil reservoirs, which was a significant limitation. This inauspicious situation has changed considerably. The Yen-Mullins model[1,2] has codified the dominant molecular and nanocolloidal structures of asphaltenes. Many diverse studies were utilized to create this model based on evidence from methods including molecular diffusion,[3–6] optics in combination with molecular orbital (MO) calculations,[7,8] high-Q ultrasonic spectroscopy,[9] mass spectrometry,[10,11] DC-conductivity,[12,13] centrifugation,[14,15] combined neutron and X-ray scattering[16,17] and aggregation dynamics vs. asphaltene concentration.[18] Subsequent to the proposal of the Yen-Mullins model, all aspects of it have been subject to examination by many techniques including NMR spectroscopy,[19–22] mass spectrometery,[23–26] and interfacial studies.[27–29] In addition, many asphaltene sample types were utilized in these studies including asphaltenes directly from crude oils of differing maturity,[4] bitumens,[19,20,30] resid asphaltene,[31] and coal-derived asphaltenes.[3,5,10,25,32–34] The comparison between petroleum asphaltenes (PA) and coal-derived asphaltenes (CDA) has been particularly informative as they differ markedly in the alkane fraction, the latter having a very small alkane fraction.

The Yen-Mullins model provides centroids, not the width, of distributions of corresponding nanostructures. These centroid structures are useful for thermodynamic modeling. The specific species (molecule, nanoaggregate or cluster) of the nanostructure model have been combined with a regular solution polymer theory to yield the Flory-Huggins-Zuo Equation of State (FHZ EoS)[35,36]

which characterizes asphaltene gradients in equilibrated oil columns, for example in oil reservoirs. Indeed, the simplicity of the asphaltenes allows for simple theoretical approaches with very few parameters.[37] The size of the particular asphaltene species (nanoaggregates or clusters) is an essential parameter required for the gravity and other terms of the FHZ EoS and, in turn, field applications set tight constraints to the possible size of the species proposed by the Yen-Mullins model. For example, the successful application of the FHZ EoS with asphaltene clusters has been established over the 100 kilometer perimeter of an oil field with a 10 times vertical variation of asphaltene concentration.[38] The cluster size used for this application sets constraints to what can be obtained experimentally, and was subsequently validated in NMR studies, which explicitly obtained an aggregation number of 6 to 7 nanoaggregates.[19] This first-principles modeling of asphaltene gradients in oil reservoirs has enabled understanding of many diverse reservoir concerns such as reservoir connectivity,[36,39,40] baffling,[41] heavy oil and tar mat formation,[38,41,42] (related to gradients of dissolved gas[43]), and viscosity gradients from diffusive processes.[44]

In a similar manner, the Yen-Mullins model has been combined with the Langmuir EoS to model three separate universal curves obtained in oil-water interfacial studies.[27–29,33] In fitting these universal curves, the only adjustable parameter is the contact area of the asphaltene molecule at the interface. In addition, these studies show that the nanoaggregate does not go to the oil-water interface in accord with its peripheral alkane chains. The requisite interfacial orientation, i.e., the asphaltene PAH in plane and the alkane groups out of plane, has been established in studies of corresponding Langmuir-Blodgett films.[45] First-principles modeling of asphaltenes in important applications reinforces the need for accurate nanostructures of asphaltenes. It remains important to verify central tenets of the Yen-Mullins model. In addition, it is important to determine the range

of distributions of these different nanostructures in the Yen-Mullins model. For example, interfacial effects can vary significantly for different molecular asphaltene structures.[46]

One topic that persistently remains subject to much debate is the asphaltene molecular architecture. Specifically, the dominance of the island molecular architecture (one PAH per molecule) has become less controversial.[19,20,23,47] The instability of archipelago structures[23] helps explain this observation as asphaltenes are stable for geologic time periods at elevated temperatures. Nevertheless, questions remain as to the relevance (if any) of the proposed archipelago structures (multiple PAHs per molecule). In particular, bulk decomposition studies of asphaltenes have shown the production of low molecular weight species containing small number of aromatic rings.[48] This has been taken as evidence for the existence of small aromatic groups attached to larger PAH cores via alkane linkages, i.e., the 'traditional archipelago' structure.[48] However, model 'island' compounds have been demonstrated to give rise to archipelago products under similar reaction conditions.[49] Evidently, bulk decomposition can lead to creation of new molecular architectures that are difficult to distinguish from the original molecular architectures. A unimolecular decomposition study[23] compared archipelago and island model compounds with asphaltenes. A large contrast was observed for all island vs. all archipelago compounds and asphaltenes were found to behave in the same way as island model compounds, not archipelago model compounds.

Recent work has provided very high resolution images of asphaltenes using atomic force microscopy (AFM) to image atomic centers and electron density at bond paths, and scanning tunneling microscopy (STM) to image the π-MOs, especially the highest occupied molecular orbitals (HOMO) and the lowest unoccupied molecular orbitals (LUMO) of individual asphaltene molecules.[50] The asphaltene PAHs provide higher quality images over those of the alkane

91 substituents, especially for carbons located further from the PAH core. Consequently, this study
92 focused on coal-derived asphaltenes to ensure optimal image clarity, since they possess a much
93 lower number of alkane substitutions. Nevertheless, PAHs of petroleum and coal-derived
94 asphaltenes could be clearly identified in each case on the basis of the MOs of their PAHs; no
95 significant difference was detected between the PAHs of petroleum asphaltenes and coal-derived
96 asphaltenes. Of the >100 molecules imaged, the island molecular architecture dominated. Not one
97 molecule with the traditional archipelago structure was found with two aromatic species bonded
98 by an alkyl linkage. A small but noticeable fraction of the molecules had two or more PAHs (or
99 aromatics) bonded directly through aryl linkages. Thus for all intents and purposes, asphaltene
100 molecules exhibited a single aromatic core, again with island architecture dominating.[50] The
101 asphaltene PAHs exhibit a large variation in the number of rings, ranging from 4 to 20 rings. This
102 diversity of asphaltene PAHs has not been detected by any other direct method; nevertheless,
103 interpretation of optical spectra by molecular orbital calculation concluded that asphaltene PAH
104 sizes vary from 4 to 15 rings.[8] In the imaging study, no aggregates were observed ruling out the
105 sequestration of an unseen fraction of asphaltene molecules. In addition, in all images randomly
106 selected areas were analyzed preventing bias. The results of the molecular imaging study provide
107 an excellent benchmark for testing new results as well as checking for consistency of earlier
108 studies.

109 Solution-state NMR spectroscopy has been a key and widely used technique in investigating
110 asphaltene structure, since it offers the advantage of studying intact molecules without the need
111 for fragmentation.[6,19,51–54] In a previous solution-state NMR spectroscopy study,[19] it was
112 demonstrated that the ‘island’ model is the dominating motif in the architecture of Athabasca
113 bitumen asphaltenes. It was shown that an average asphaltene molecule consists largely of a single

PAH core, with ~6-7 pericondensed aromatic rings. Alicyclic groups were shown to be condensed to the aromatic core, and the presence of clusters consisting of 6 to 7 nanoaggregates was reported. In a separate solution-state NMR spectroscopy study, Andrews *et al.*[21] compared five different asphaltenes, three coal-derived (CDA) and two petroleum (PA) derived, which also support the island architecture. It was also shown that both PA and CDA have approximately 6 fused rings per aromatic cluster. The aliphatic chain length distribution was shown to be quite large for both, with PA having a higher fraction of aliphatic carbons in longer chains.

Solid-state NMR spectroscopy has also found a fair amount of use in structural studies of asphaltenes, but most of the techniques employed have been rudimental in nature.[51,52,55–63] In a previous solid-state NMR study of Athabasca bitumen asphaltenes, Dutta Majumdar *et al.*[20] noted that some previous investigations using solid-state NMR spectroscopy improperly quantified the carbon species in asphaltenes, neglecting the underlying narrow signals in an otherwise broad spectrum.[52,59] The study by Dutta Majumdar *et al.*[20] verified the structural motif of asphaltenes occurring in clusters of interlocking nanoaggregates, where alkyl side chains of adjacent aggregates are intercalated between aromatic stacks.[20] It was also noted that when single contact time cross-polarization (CP) experiments are used, quantitative results are unlikely and directly polarized (DP) ^{13}C experiments are required. Recent work by Alemany *et al.*[64] using solid-state NMR spectroscopy thoroughly reviews some of the pitfalls of CP based techniques and note that only certain petroleum asphaltenes provide quantitative CP spectra. However, solid-state NMR literature of asphaltenes appears to lack an example where a proper analytical CP-dynamics model was used for quantification. Storm *et al.*[52] provides one of the earliest CP-dynamics studies, reporting cross-polarization time-constants (T_{CP}) and ^{1}H spin-lattice relaxation time in the rotating frame ($T_{1\rho H}$), which are useful parameters required to understand molecular structure and

dynamics. However, doubt may be raised about the CP-dynamics model used by Storm to arrive at these values, which is different from the established models in solid-state NMR spectroscopy literature.[65] Pekerar *et al.*[59] also reported T_{CP} values but the CP-dynamics model used was not mentioned, neither were the CP-dynamics discussed in detail. The interpretation of the T_{CP} data was based only on segmental mobility arguments, which is not wrong, but is incomplete, as shall be demonstrated. Moreover, for complex polyaromatic systems such as asphaltenes, the conventional single ^{1}H spin-bath CP dynamics model does not provide the best fit to the experimental data, as shall be demonstrated later in this work.

To the best of our knowledge, a solid-state NMR spectroscopic study comparing PA and CDA has not been reported to date. Such a study is important at this juncture, especially in the light of important observations made in the recently reported AFM images of PA and CDA.[50] The work presented herein illustrates how solid-state ^{13}C NMR spectroscopic techniques can be used to compare the structural hierarchy of a PA and a CDA. It is known that asphaltenes derived from coal distillates are structurally distinct from those derived from petroleum.[21] CDA are posited to be less complex than their petroleum counterparts, owing to the manner in which they are processed from liquefied coal resids by distillation, which leads to the cracking of the alkane chains.[21] Coal-derived asphaltenes are consistently of lower mass and smaller size than petroleum asphaltenes, likely making them structurally less complex and thereby easier to study.[66] A refined model for CP dynamics suited for these systems will be presented and its suitability for quantification of carbon types will be tested by comparing the results with quantitative DP ^{13}C experiments. This CP model is better-suited for asphaltene characterization, and is richer in structural information, compared to what has been employed previously for the same purpose.[20] A domain selective technique, refocused DIVAM (Discrimination Induced by Variable Amplitude

Minipulses), will be used to distinguish the signals from environments differing in mobility, which highlight key differences between the two types of asphaltenes. These techniques were able to shed light on several structural features, such as the size of the aromatic core, alkyl chain length, the nature of the aggregates in the two asphaltenes and the aliphatic-aromatic interactions that influence the mobility of certain groups, which are key to understanding the role of asphaltene structure on aggregation behavior. Finally, optical absorption measurements were performed to assess the differences and similarities of the PAH distributions for PA and CDA for comparison to results obtained from NMR spectroscopy.

2. Theoretical background

2.1. ***^{1}H-to-^{13}C Cross-Polarization (CP) Dynamics****:* The details of the cross-polarization (CP) technique are well documented in literature[67] and we have described the technique in a previous work.[20] In brief, CP is used to enhance the signals from low natural abundance nuclei such as ^{13}C by transferring magnetization from an abundant nucleus in the system, such as ^{1}H, via heteronuclear dipolar coupling. It also results in significant reduction in experimental time requirements, since the timescale of CP experiments is governed by the ^{1}H longitudinal relaxation delay (T_1) rather than that of ^{13}C, which is often an order of magnitude longer. The rate of build-up of the cross-polarized ^{13}C signal is dependent on the effective heteronuclear dipolar coupling between the carbon in question and its neighboring hydrogens (protons). The strength of the dipolar coupling is affected by the spatial proximity of the nuclei (^{13}C and ^{1}H) to each other and by the mobility of the groups involved in the polarization transfer.

Cross-Polarization Models: The build-up of the ^{1}H-to-^{13}C CP magnetization and eventual decay is traditionally described by the two-spin thermodynamic *I-S* model, described by the following equation:[65]

$$I_t = I_0 \times \lambda^{-1} \times \left(1 - \exp\left(-\frac{\lambda t}{T_{CP}}\right)\right) \times \exp\left(-\frac{t}{T_{1\rho H}}\right) \quad \text{Equation 1}$$

where I_t is the experimental intensity of the cross-polarized ^{13}C magnetization at a contact time t, I_0 is the equilibrium carbon magnetization and $\lambda = 1 - \frac{T_{CP}}{T_{1\rho H}}$. T_{CP} is the cross-polarization transfer time constant that governs the build-up portion of the CP dynamics curves while the decay part of the curves is governed by $T_{1\rho H}$ or the rotating-frame spin-lattice relaxation time constant of ^{1}H. In this model the inherent assumption is that the ^{1}H spin-diffusion through the system occurs fast enough so that all the carbons spins (*S*) are polarized by a single proton spin-bath (*I*).[65] All other factors being equal, a shorter ^{1}H-^{13}C distance means a stronger dipolar interaction, which facilitates faster magnetization build-up and hence shorter T_{CP} values. The shortest T_{CP} values are usually seen for carbons which have directly attached protons, except highly mobile moieties such as –CH_3 where the dipolar coupling is averaged. T_{CP} can get exceptionally long for carbons which do not have directly attached protons, such as quaternary and carboxylic carbons.

However, it has been shown that for complex materials such as soil- and coal-humic acids, the single proton-spin-bath assumption does not hold. A non-monotonic cross-polarization model, described by Equation 2, which allows for two different proton-spin-baths, provides a better fit to the experimental data.[68]

$$I_t = I_0 \times \left(1 - \frac{1}{2}\exp\left(-\frac{t}{T_{CP1}}\right) - \frac{1}{2}\exp\left(-\frac{3t}{2T_{CP2}}\right) \times \cos\left(\frac{bt}{2}\right)\right) \times \exp\left(-\frac{t}{T_{1\rho H}}\right) \quad \text{Equation 2}$$

All the terms in Eq.2 have the same meaning as Eq. 1. T_{CP1} and T_{CP2} are the cross-polarization time constants associated with two different ^{1}H spin-baths (*vide infra*), $b = \frac{\gamma_H \gamma_C \hbar}{2r_{C\text{-}H}^3} \times (3\cos^2\theta\text{-}1)$ is the ^{13}C-^{1}H dipolar coupling parameter (in radians/s) which contains the ^{1}H and ^{13}C gyromagnetic ratios (γ_H, γ_C), ^{1}H-^{13}C distance $r_{C\text{-}H}$ and the $(3cos^2\theta - 1)$ term that connect dipolar coupling and chemical shift anisotropy.

Equation 2 represents the *I*-*I**-*S* model where two different sized proton spin baths are assumed. The first is the smaller spin bath I^* which represents protons in close proximity to the carbon (S) spin bath of comparable magnitude, and the I^*-*S* pair exchange magnetization in an oscillatory manner. This oscillatory exchange is damped by spin-diffusion from the larger spin-bath denoted by *I*, representing the bulk of the protons at a larger distance from the carbons.[65] The CP time constant T_{CP1} represents the initial magnetization transfer at short contact periods (t), from protons that are closest to the carbon spins (not necessarily attached). This magnetization transfer occurs rapidly (short T_{CP1}) between contiguous protons and carbons, with strong dipolar coupling. For quaternary or carboxylic carbons, the dipolar coupling is weaker due to no attached protons, leading to slower CP transfer (long T_{CP1}). A slower CP transfer can also occur in a mobile environment. As the contact period is incremented, another CP mechanism, characterized by T_{CP2}, takes over. It is facilitated through energy exchange with the whole ^{1}H spin-system via proton spin-diffusion, which in turn is predicated on segmental motion within the molecules.[68,69] This mechanism is likely active from the onset of the contact period, but its effect is less evident when the dipolar coupling of the carbons with the closest protons is strong. Larger segmental motion interferes with spin-diffusion and weakens the effective dipolar coupling, which leads to a longer T_{CP2} values. If the overall ^{1}H spin bath is larger, T_{CP2} values can be expected to shorter due to more effective spin diffusion. This spin-diffusion mechanism also becomes a lot less effective at “fast”

MAS speeds. “Fast” MAS can be defined as speeds which are much faster than the natural ^{1}H linewidth and can narrow the ^{1}H signals. All the experiments in this paper were carried out at 8 kHz MAS, which is small compared to the very broad ^{1}H solid-state NMR signal of asphaltenes,[20] thus the spin-diffusion mechanism of polarization transfer can be safely assumed to be effective.

The inverse of the T_{CP} time constants or the CP rates (R_1 for T_{CP1}, R_2 for T_{CP2}) provides a measure of the scaling of the theoretical single bond C-H dipolar coupling (D_{CH}), which reflects the distance of the carbon nuclei of interest to the ^{1}H spin-bath and its segmental mobility. A typical D_{CH} for a C-H spin pair with an internuclear distance of 1.10 Å, in the absence of any motional averaging, is 22.7 kHz. If the cross-polarization rate is comparable to this value of D_{CH}, it implies directly bonded C-H pairs with no or little motional averaging. A significant scaling down of the CP rates could result from increased distance between the carbon nuclei and the proton spin bath, or segmental motion, or both.

2.2. *Pre-CP Refocused Discrimination Induced by Variable Amplitude Minipulses (DIVAM)*:

The Refocused DIVAM experiment[70] was originally introduced as an improvement on the DIVAM[71–73] experiment, designed for domain selection in fluoropolymers. These sequences can selectively excite signals from mobile, disordered domains or rigid, ordered domains by exploiting differences in their T_2 behavior and strength of dipolar coupling. In a previous work[20] we show how the CP variant of the DIVAM sequence can be used to distinguish rigid and mobile domains in asphaltenes. The CP refocused DIVAM is similar, but with added refocusing pulses between the minipulses to remove coherent dephasing due to heteronuclear coupling and chemical shift evolution. It reduces the phase distortions and offset dependence associated with non-refocused

DIVAM, and allows the selection to be governed by T_2 rather than T_2*.[74] The mode of action of this sequence, and its differences with DIVAM has been discussed in details elsewhere.[70] In brief, the CP refocused DIVAM sequence consists of a repeatable loop of four pulses on the ^{1}H channel: 2 × low-amplitude (≤90°) r.f. pulses, 2 × refocusing pulses, separated by interpulse delays of fixed duration. This is followed by a standard ^{1}H-to-^{13}C CP sequence, where the ^{1}H magnetization remaining after the refocused DIVAM filter is transferred to ^{13}C (hence "pre-CP"). Typically, in what is referred to as a "nutation" experiment, the excitation angle is incremented in fixed steps from 0° to 90° by gradually increasing the pulse widths of the low-frequency r.f. pulses, and the signal intensities are plotted against the excitation angle. These plots, called nutation curves, reflect the mobilities of the respective moieties and, thus, enable the differentiation between signals from rigid or mobile components. The nutation curves for the more mobile components show pronounced oscillations in intensity and usually have a zero crossing at smaller excitation angle. Conversely, the rigid components have nutation curves which are comparatively damped and zero crossing occurs at larger angles, if at all. Although the final observation is done on ^{13}C, since the filtering is performed on the ^{1}H nucleus, in essence the nutation curves represent the mobilities of the protons from which the CP is occurring. This will be an important fact to remember while we discuss the nutation curves.

3. Experimental section

3.1. *Asphaltene extraction*

The petroleum asphaltenes (UG8) were extracted from crude oil by standard n-heptane precipitation. Briefly, n-heptane was added 40:1 to the crude oil, and the mixture was stirred

overnight to allow the asphaltenes to precipitate. Precipitates were then extracted by vacuum filtration over a Teflon membrane with 0.47 micron pores. Co-precipitates were removed by Soxhlet extraction with n-heptane for three days. The Wyoming coal asphaltenes (WY) were obtained from solid residues from distillation of coal extracts in coal liquefaction plant, as described previously.[21] The asphaltene fraction, which is toluene soluble and n-hexane insoluble, was obtained by Soxhlet extraction.

3.2. *Solid-state NMR Spectroscopy*

All CP experiments were performed at the University of Lethbridge, on an 11.74 T Bruker Avance III HD dedicated solid-state NMR spectrometer (499.85 MHz ^{1}H and 125.67 MHz ^{13}C frequencies) equipped with four RF channels, using a 4.0 mm MAS quadruple resonance probehead with a 53 μL rotor, at a spinning speed of 8 kHz and ramped-amplitude Hartmann-Hahn matching. Higher spinning speeds were considered to reduce the effect of spinning sidebands, but it greatly reduces CP efficiency. A recycle delay of 2.0 s was used for all CP experiments and a 3.0 μs 90° pulse-width was used for ^{1}H. Other than the variable contact time experiments (CP dynamics study), all other CP experiments were performed with a contact time of 0.8 ms for UG8 PA and 1.0 ms for WY CDA, which visually provided the optimum intensities for all the observable peaks. 2048 scans were recorded each variable contact time experiment and a 50 Hz exponential line broadening was used to improve the signal-to-noise ratio at the expense of resolution. The ^{1}H and ^{13}C spin-lock field used for all CP experiments was 55.6 kHz, with a ramped amplitude Hartmann-Hahn match. The DP ^{13}C experiments were performed at a MAS speed of 16 kHz using the same instrumental set up as above, with a recycle delay of 90 s was used to allow the magnetization to completely return to equilibrium. The ^{13}C 90° pulse-width was 2.5 μs for the DP experiments. Broadband ^{1}H decoupling was used for all experiments.

291 The pre-CP refocused DIVAM filtering sequence consists of a repeatable block of four pulses
292 on the ^{1}H channel: 2 × low-amplitude (≤90°) r.f. pulses, 2 × refocusing π-pulses, separated by
293 interpulse delays of fixed duration which was automatically calculated by rotor-synchronization
294 to 8.0 kHz. The block was repeated 4 times for each experiment and the pulse powers used
295 corresponded to a 3.0 μs 90° pulse on ^{1}H. Following the filtering sequence the magnetization was
296 cross-polarized to ^{13}C using the exact same conditions as the CP experiments. A series of 19
297 measurements were carried out by increasing the excitation angle of the low-amplitude
298 'minipulses' in 5° steps from 0° to 90°, with 1024 scans at each step, and the peak areas were
299 plotted against the excitation angles.

300 All spectral processing, deconvolution and analysis were done using the MestreNova software
301 (v 9.0.1). The CP dynamics parameters were obtained by fitting the experimental curves with CP
302 dynamics equation (*vide infra*) on the statistical software Minitab 17, using a Levenberg-
303 Marquardt[75] non-linear regression algorithm. The standard errors for the parameters obtained from
304 CP were calculated by the software with a 95% confidence interval.

305

306 **3.3. *Optical Spectroscopy***

307 Visible-NIR spectra were obtained using a Cary 5000 UV-Vis-NIR spectrometer. Samples were
308 placed in a 500 μm path length cuvette. Asphaltene samples were dissolved in carbon tetrachloride
309 and sonicated for 3 hours and allowed to sit overnight prior to spectroscopic measurements.
310 Spectra were collected over the range of 250 –3,300 nm. Background signal was collected as pure
311 solvent and subtracted. Spectra were baseline corrected for wavelength-independent scattering.

312 Data was normalized to mg of aromatic hydrocarbon per gram of solvent, using the aromaticities
313 presented below.

314

315 **4. Results and Discussions**

316 The elemental compositions of UG8 PA and WY CDA have been published previously.[21] The
317 principal differences are the much higher sulfur (S) content (8.94%) and a higher H:C atomic ratio
318 (1.05) of the UG8 PA, compared to 0.13% S and a H:C ratio of 0.81 in the WY CDA.

319

320 **4.1. *Spectral deconvolution***

321 Figure 1 shows the deconvolution models for the ^{13}C CP NMR spectra of UG8 and WY
322 asphaltenes obtained under 8 kHz MAS. The starting point of constructing the models was the
323 fitting model used in our previous solid-state NMR spectroscopy study.[20] Since these samples are
324 different from the one used in the previous study,[20] all the chemical shifts and linewidths had to
325 be adjusted to provide the optimum fit. Peaks were added at chemical shifts where shoulders or
326 features were observed. For example, in the UG8 NMR spectrum (Fig. 1), the peak at 31.98 ppm
327 was added to account for the obvious shoulder (i.e. not an artifact) present on the most intense
328 aliphatic signal around ~30 ppm. Whether an obscure spectral feature is a real signal or an artifact
329 was determined by checking if it is consistent between the spectra at different contact times. The
330 spinning sidebands were placed such that they are separated from the corresponding centerband
331 by an integer multiple of around ~64 ppm (= 8 kHz/125.67 Hz), and their linewidths were kept the
332 same as the centerband. It is important to note here that the assignments, especially for the broader
333 fitted peaks, are not solely based on the isotropic chemical shift value, but also on their linewidths,

since most of them span a range of several ppm. For example, the peaks at ~138 ppm in the spectra of both asphaltenes are assigned to both substituted aromatic carbons and double bridgehead carbons, even though ~135 ppm is generally regarded as cut-off for bridgehead carbons, which appear upfield of this chemical shift. It is clear in Fig.1 that these peaks span upfield of 135 ppm,[64] which justifies the double assignments. A total of 15 and 11 isotropic peaks were fitted to the UG8 and WY spectra, respectively, in addition to 10 spinning sidebands in UG8 and 15 in WY. The deconvolution models, along with details of the fitting parameters such as linewidths and Lorentzian/Gaussian (L/G) lineshape ratios, are provided as Supplementary Information. For the DP spectra (see Supporting Information), the same fitting model was used, but with an additional peak in the aromatic region and the peaks from the probe background (*vide infra*). A depiction of the different types of carbons assigned is provided in Fig. 2 along with their description in Table 1, while the assignments for each fitted isotropic peak can be found in Table 2 (UG8) and Table 3 (WY). Energetic considerations about different structures have been discussed elsewhere.[76] Not much information can be gathered from comparing a single spectrum of each kind of asphaltene, other than the obvious conclusion that WY CDA have a larger aromatic fraction and smaller aliphatic fraction. It would also be unwise to perform quantitative calculations on these two spectra since CP spectra of complex polyaromatic hydrocarbon (PAH) systems are inherently non-quantitative.[20] To obtain more meaningful and possibly quantitative information, the build-up of carbon magnetization over increasing contact time, or the CP dynamics, has to be studied, and then compared to the corresponding information from the DP experiments. The CP dynamics curves are shown in Fig. 3 and the following section discusses them in detail.

4.2. *CP Dynamics*

The curve fitting for the variable contact time data was initially done using both Eq. 1 and Eq. 2, but on comparison Eq. 2 was found to provide a better fit, especially in cases where the build-up portion of the curves shows two distinct components (for an example fitting comparison, see Supplementary Information). Hence, Eq. 2 will be used to study the CP dynamics in this paper.

Fitting results: In Table 2 and Table 3, we present the cross-polarization parameters (T_{CP1}, R_1, T_{CP2}, R_2, $T_{1\rho H}$ and b) obtained by fitting the experimental data with the non-monotonic CP model (Eq. 2) for UG8 and WY asphaltenes, respectively. Certain low-intensity peaks, such as the 147.51 ppm signal in UG8 (R_1 = 33.3 ± 33.3 kHz) and the 111.59 ppm (R_2 = 11.1±9.9 kHz) signal in WY, have large errors associated with at least one of their calculated parameters, and their overall contribution to the spectrum is minor, making them unusable to obtain structural information. The ipso-carbons bonded to heteroatoms, (C_{sub}-O-C, C_{sub}-N, C_{sub}-OH) (UG8: 162.51 ppm, WY: 155.54 ppm), also have a minor contribution to the overall spectrum, and hence will not be used to draw any major conclusions. It is the most intense peaks in the spectra (Fig.1) that provide the most robust analysis and important results, and the discussions will be primarily focused on these. The alkyl substituted (C_{sub}-R) and double bridgehead (C_{db}) aromatic carbons (UG8: 138.02 ppm, WY: 138.31 ppm) exhibit significantly reduced R_1 (4.0 ± 0.8 and 4.5 ± 0.8 kHz respectively) because of no attached or nearby hydrogens. The 127.44 ppm signal in WY coal asphaltenes has a large R_1 (25.0 ± 6.3 kHz) which indicates that a significant fraction of aromatic –CH ($C_{H,ar}$) groups resonate in this region, unlike the corresponding 129.28 ppm UG8 signal with a significantly smaller R_1 of 8.3 ± 0.7 kHz, justifying its assignment only to double and triple bridgehead carbons. The reduced R_2 of both the 127.44 ppm (WY) and 129.28 ppm (UG8) signals, at 0.2 ± 0.1 and 1.0 ± 0.1 kHz

379 respectively, are due to the triple bridgehead carbons (C_{tb}), which are remote from the ^{1}H spin-
380 bath.

381 The 122.52 ppm signals of WY and the corresponding 123.78 and 118.53 ppm signals of UG8,
382 all have moderately large R_1 and R_2, both the values being similar, in the range 14-20 kHz, which
383 means that the dipolar coupling mechanism of CP dominates over spin-diffusion, and that these
384 signals are mostly from $C_{H,ar}$ groups. The majority of the $C_{H,ar}$ of UG8 resonate in the 118-124
385 ppm region indicating large number of alkyl substitutions, which decrease the chemical shift of
386 adjacent $C_{H,ar}$ groups from the base benzene shift of 128.6 ppm. Conversely, WY CDA aromatic
387 carbons are substituted to a lesser extent, evinced by the higher chemical shift (127.44 ppm) of a
388 significant fraction of the $C_{H,ar}$ groups. The lower chemical shift $C_{H,ar}$ groups also represent 'bay'
389 type configurations, while those at the higher (>125 ppm) represent 'fjord' type configurations[77]
390 (see Fig 2 and Fig. S3 in the Supplementary Information for examples), which shows that while
391 'bay' regions are present on both the asphaltenes, only WY CDA have 'fjord' motifs. These 'bay'
392 and 'fjord' motifs were also observed by Schuler *et al.*[50] in their recent work using AFM imaging.
393 Moreover, the chemical shifts of $C_{H,ar}$ groups closer to 130 ppm are characteristic of small aromatic
394 rings which are covalently tethered to a larger PAH, as seen in hexabenzocoronene derivatives.[78,79]
395 This observation shall be investigated further in a subsequent section.

396 The UG8 signal at 109.58 ppm exhibits a moderately low R_1 value of 5.3 ± 2.2 kHz, suggesting
397 that it could be from non-protonated carbons. However, the chemical shift fall strictly within the
398 $C_{H,ar}$ range, which makes the assignment difficult. Simply going by the CP build-up curve (Fig.
399 3), it appears to build up much more rapidly than other quaternary carbons, which indicates that it
400 is most likely $C_{H,ar}$ groups. The dominating CP mechanism here appears to be the ^{1}H spin-
401 diffusion, hence the high R_2 value in UG8 (16.7±5.6 kHz) which has a large overall ^{1}H spin bath.

All the terminal aliphatic carbons, and the ones which are α, β or γ from the free end of a sidechain, exhibit significantly reduced R_1 values in the range 4.8 ± 0.1 to 11.1 ± 2.5 kHz for the UG8 asphaltenes, compared to those in WY asphaltenes, in the range (11.1 ± 7.4 to 25 ± 6.3 kHz) (UG8: 14.30, 22.71, 29.77 ppm, WY: 14.36, 22.88, 29.82 ppm). This is a strong indicator of the UG8 asphaltenes possessing longer, hence more mobile aliphatic sidechains, which diminishes the effective dipolar coupling and reduces CP efficiency. The isobutyl -CH_3 or -CH_2 groups α to terminal -CH_3, and the groups in the middle of the chain (UG8: 22.71, 29.77 ppm, WY: 22.88, 29.82 ppm) also show smaller R_2 values in UG8 (0.8 ± 0.5 to 12.5 ± 6.3 kHz) compared to those on WY (2.9 ± 0.7 to 25 ± 12.5 kHz), which suggests that ^{1}H spin-diffusion is disrupted by segmental motion, corroborating the above statement. The methyl groups directly attached to the aryl rings, and branched methyl groups in WY asphaltenes (19.38 ppm) have a larger R_1 of 25.0 ± 6.3 kHz, compared to the 14.3 ± 1.0 kHz R_1 in UG8 (19.64 ppm). This is a result of WY asphaltenes having a larger aromatic ^{1}H spin-bath and shorter sidechains (shown quantitatively later), which results in these methyl groups being very close to the aromatic core, with a less mobile environment. The contribution of branched methyl groups to the 19.38 ppm signal in WY is likely quite low, due to the alkyl sidechains being quite short. The broad UG8 peak at 29.59 ppm exhibits large and similar R_1 and R_2 values, 14.3 ± 2.0 and 20 ± 4.0 kHz, respectively, which is coherent with its assignment to alicyclic -CH_2 groups and chain –CH_2 groups α to aryl rings. The rigidity of these groups allow fast magnetization build-up through predominantly the dipolar coupling mechanism.

One of the overall differences between the aliphatic carbon signals of UG8 and WY asphaltenes is that in UG8, most of the signals are comparatively narrower (smaller linewidth) than their WY counterpart, except those assigned to alicyclic groups. A narrower linewidth is characteristic of

greater mobility. Also, the comparison of the CP build-up curves (Fig. 3) show that the decay of magnetization due to ^{1}H spin-lattice relaxation in the rotating frame starts occurring earlier in UG8 aliphatic signals across the board. This is evidence that ^{1}H spin-diffusion is less effective for the UG8 sidechains, likely due to the higher degree of local mobility in them, which is a direct consequence of longer chain lengths. From the assignments, it can also be seen that UG8 asphaltenes have a significantly larger alicyclic fraction and sulfur functionalities, which is consistent with the elemental analysis (UG8: 8.94 wt% S, WY: 0.13 wt% S).[21]

4.3. Quantification using CP dynamics and DP ^{13}C spectra

From the variable contact time CP experiments, the percentages of the different types of carbon (%*C*) were calculated using Eq. 3:

$$\%C = \frac{I_0^i}{\Sigma I_0^i} \times 100 \qquad \text{Equation 3}$$

where I_0^i is the equilibrium magnetization of the i^{th} fitted peak, the value of which was obtained by fitting Eq. 2 to the variable contact time data. Equations 1 and 2 can provide a quantitative I_0 only when the basic CP condition, $T_{CP} < T_{1\rho H}$, is valid as in this case. In other words, if the ^{1}H spin-lattice relaxation in the rotating frame starts before the completion of ^{1}H to ^{13}C magnetization transfer, Eq. 2 (or Eq. 1) cannot be used to study CP dynamics.

Recall that the fitted peak at ~ 138 ppm for both the spectra was assigned to both C_{sub} and C_{db} because of their broadness. The relative contribution of C_{sub} to the peak area was determined by calculating the area between 135 and 160 ppm under a Lorentzian peak centred at ~138 ppm (UG8: 138.02 ppm, WY: 138.31 ppm), with the corresponding full-width at half maximum (i.e.

446 linewidth). This allowed the determination of the percentage of the area under the peak
447 corresponding to C_{sub}, and the remaining was assigned to C_{db}. For UG8, the C_{sub} contribution to
448 the 138.02 ppm peak was calculated to be ~79%, while for WY the C_{sub} contribution to the 138.31
449 ppm peak was ~76%. Using Eq. 3, the percentages of aromatic (UG8: 47.2 ± 2.4%, WY: 81.2 ±
450 2.3%) and aliphatic (UG8: 52.8 ± 6.5%, WY: 18.8 ± 5.5%) carbon in both the asphaltenes were
451 found to be reasonably close to the values observed previously via solution-state NMR techniques
452 for the same samples.[21] If the solution-state results are indeed quantitative, the similarity in the
453 aromaticity values make the CP method appear promising. However, the CP dynamics based
454 calculations should be compared with those obtained from the DP ^{13}C spectra, which are generally
455 regarded as more quantitative in the solid-state. For this purpose, the DP ^{13}C spectra of both
456 asphaltenes, obtained at 16 kHz MAS to eliminate sidebands, were also deconvolved (Fig. S4,
457 Supplementary information), using the same deconvolution model, with additional peaks fitted
458 wherever necessary. Extra aromatic carbon peaks centred at ~121 ppm, had to be fitted to the DP
459 ^{13}C spectrum of both asphaltenes, which clearly shows that certain quaternary carbons remain
460 underestimated by CP methods. One aspect of DP spectra collected using long relaxation delays
461 that is often overlooked, is the occurrence of background signals from the probe, which is not a
462 significant concern in CP, where probe background is eliminated by the phase cycling, which is
463 not possible in DP.[80] An empty rotor was used to collect the background signals, which were then
464 taken into consideration while fitting the DP spectra (Fig. S4, Supplementary information). The
465 majority of these background signals appear under the aromatic region of the asphaltene, and can
466 lead to overestimation of the aromaticity if not accounted for. Even when the background signals
467 are accounted for, uncertainty persists in the aromatic region, especially when the signal-to-noise
468 ratio (S/N) is very low, which is usually the case for DP. Sufficient signal-to-noise ratio, at least

469 at the level of the CP spectra would require weeks of time or larger rotors, which again limits
470 spinning speed. Furthermore the aliphatic contribution can be significantly underestimated with
471 spinning sideband overlap, even with the 16 kHz spinning in this case. Here the spinning rate
472 could not be increased further to prevent overlap due to the rotor size (4 mm). Lower spinning rate
473 ca. 7 kHz may minimize the problem in this case, however, at the cost of resolution. Again, smaller
474 rotors would be required to spin faster dramatically reducing the S/N per unit time, hence
475 mandating weeks of experiment time. Only a lower field strength will help in this case, where
476 spinning sideband will be much smaller and will not overlap with the signals of interest.

477 Based on the CP and DP data, certain important structural parameters were computed,
478 which are listed in Table 4. They are best described in a comparative manner. The fraction of
479 aromatic carbons (aromaticity) in UG8 calculated using the DP spectra (64.2 ± 0.5%)came out to
480 be higher than that calculated using CP (47.2 ± 2.4%). It is expected, since CP likely cannot excite
481 those quaternary carbons that are far removed from the ^{1}H spin-bath. However, as discussed above,
482 there is always a significant degree of uncertainty associated with the aromatic region of the DP
483 spectrum due to the probe background signal, which may lead to overestimation the aromaticity.
484 Nevertheless, more quaternary carbons are expected to be observed in the DP spectrum, and for
485 large PAH systems these would be mostly the triple bridgehead aromatic carbons (C_{tb}). Most of
486 this increase in aromaticity can be attributed to the additional peak that was fitted in the UG8 DP
487 spectrum (121.17 ppm). The chemical shift prompts an assignment mostly to C_{tb}, since $C_{H,ar}$ groups
488 would have been detected in the CP spectrum. For the WY CDA, however, the aromaticities
489 estimated by CP and DP are almost equal (CP: 81.2 ± 2.3%, DP: 82.1 ± 0.1%). To understand why
490 this is the case, the fraction of each type of aromatic carbon needs to be investigated. For the WY
491 CDA, the $C_{H,ar}$ fraction is significantly larger when obtained from CP (17.8 ± 2.6%) than that from

492 DP (10.1 ± 0.0%), whereas the $C_{H,ar}$ fraction of UG8 is the same from both techniques (CP: 13.3
493 ± 6.4 %, DP: 13.4 ± 0.2%). The CP experiments, given their reliance on the distance between the
494 ^{1}H and ^{13}C spin-baths, are likely to better represent, quantitatively, smaller ring systems with a
495 large $C_{H,ar}$ fraction. Therefore, in the WY CDA, there must be a significantly larger fraction of
496 smaller PAHs (2-4 rings) that themselves have a larger $C_{H,ar}$ fraction, which raises its average
497 aromaticity obtained from CP, even though the bridgehead carbons are underestimated by the
498 technique. This fraction of smaller PAHs appears to be less abundant for the UG8 asphaltenes,
499 given that the $C_{H,ar}$ fraction was found to be equal in both the CP and DP spectra. The additional
500 aromatic peak was fitted to the WY DP spectrum at 121.40 ppm was also assigned to quaternary
501 C_{tb} groups. For both asphaltenes, the bridgehead groups (C_{db} + C_{tb}) were found to be the most
502 abundant form of aromatic carbon (UG8: 33.8 ± 0.3%, WY: 46.3 ± 0.1%) using DP, and also using
503 CP (UG8: 18.5 ± 3.6%, WY: 35.3 ± 3.9%), indicating that large PAHs dominate in both.

504 The aromatic condensation index, χ_b,[21,81] is usually calculated by dividing the fraction of
505 bridgehead carbons by the aromaticity and provides a measure of the average PAH size. Based on
506 the CP calculations, the χ_b for both asphaltenes was determined to be 0.40 ± 0.02, which
507 corresponds to PAHs consisting of ~20 aromatic carbons or 5 rings. As discussed above, CP clearly
508 underestimates the bridgehead carbon fraction (C_{db} + C_{tb}). Therefore, these χ_b values are more
509 biased towards smaller ring systems, with a lower fraction of bridgehead carbons. Moreover,
510 bridgehead carbons in these smaller PAHs are also more exposed to the ^{1}H spin bath, compared to
511 those in larger PAHs. These ring sizes can thus be considered as the average for the smaller
512 asphaltene PAHs, with the larger PAHs detectable only through DP ^{13}C NMR spectroscopy. The
513 χ_b values calculated from the DP spectra were 0.53 ± 0.30 and 0.56 ± 0.06 for UG8 and WY
514 asphaltenes, respectively, that are in good agreement with reported values for the same

asphaltenes.[21] These values correspond to PAHs consisting of greater than 7 to 9 pericondensed rings in both asphaltenes. It is worthwhile noting here that these PAH sizes represent the average molecule, i.e. the actual molecules span a range of sizes, from smaller than 5 rings to greater than 9 rings. Comparing the parameters obtained from the CP and DP experiments allows us to shed some light on this size distribution, as shown above, with the WY CDA possessing a relatively larger fraction of the smaller PAHs and the larger PAHs being the dominant motif (bridgehead carbons are by far the most abundant aromatic species, Table 4). The CP results indicate that even among the comparatively smaller PAHs, the bridgehead carbons are most abundant, suggesting dominance of pericondensed structures. The dominance of the larger PAHs has been recently observed through direct molecular imaging using atomic force microscopy (AFM)[50] and is supported by these results. Assuming a single PAH core per molecule, the larger PAHs corresponds to the high mass tail for asphaltenes as reported in mass spectroscopic studies.[82] The important implication is that the molecular architecture found in the high mass tail matches that of the bulk, the island architecture.

Generally the average sidechain length is calculated by dividing the total aliphatic content by the number of aliphatic substitutions, the latter being considered a representative for the number of sidechains. However, substitutions can be of both chain and cyclic type. Therefore, terminal $-CH_3$ groups are likely to be better representatives for the number of sidechains. The average chain lengths calculated in this manner from the DP spectra were between 5.5 and 10.7 for UG8, and between 2.7 and 4.9 for WY, commensurate with the prevailing notion that petroleum asphaltenes possess longer alkyl chains. The chain lengths were overestimated in CP (UG8: 10.7, WY: 4.9), possibly due to the underestimation of the aromatic fraction, which inadvertently results in an apparently higher aliphatic fraction than in the DP spectra. Andrews *et al.*[21] reported that CDA

538 have a small fraction of alkyl chains that are at least 9 carbons long, but evidence for such long
539 chains was not found in this work, although the above-stated conclusion cannot be completely
540 ruled out since the experiments by Andrews *et al.*[21] were performed in the solution state, which
541 offers better resolution. However, AFM imaging results have shown that CDA are unlikely to have
542 such long chains.[50]

543 These calculated parameters, along with a few others are listed in Table 4 and average
544 structures constructed on the basis of these parameters are presented in Fig. 4. While constructing
545 the models, effort was taken to maintain the H:C atomic ratio close to that obtained from elemental
546 analysis. Two different PAH sizes for each type of asphaltene are shown, to represent the range of
547 χ_b. The chemical formula, molecular weight, and elemental analysis of each model is also provided
548 in the figure. The assumption that the single core motif dominates asphaltene structure is based on
549 the aromatic condensation index χ_b and the large fraction of double- and triple-bridgehead carbons.
550 These values indicate that pericondensed cores with >9 aromatic rings constitute a large PAH
551 core. If two or more of these PAHs (consider those in Fig. 4) are linked together via alkyl chains,
552 and if this motif is considered to be the dominating architecture (i.e. the archipelago model), the
553 average molecular weight, and the corresponding weight range for these asphaltenes would be
554 much higher than what has been reported based on mass spectrometric techniques that do not cause
555 fragmentation.[23,82–84] For instance, if two or more of the hypothetical UG8 molecules of Fig. 4 are
556 linked together via alkyl linkages, the molecular weight of the system will be easily > 2000 u,
557 which cannot be the average motif, since non-fragmenting mass spectroscopic studies consistently
558 report average weights of < 1000 u.[23,66] An average molecule consisting of a single-core, and at
559 most a small pendant aryl-linked aromatic system, is more consistent with the reported molecular
560 weights. Moreover, unimolecular decomposition studies are inconsistent with this traditional

archipelago structure.[23,26] Additionally, the recent AFM imaging results from Schuler *et al.*[50] have to date not found a single molecule with this traditional archipelago structure. From these practical considerations, it seems unlikely that the "traditional archipelago" structures have any significant contribution to the overall architecture of asphaltene molecules, and the average structure consists of a single core. By 'traditional archipelago' we refer to those proposed by Sheremata *et al.*[85] However, such archipelago structures cannot be ruled out completely, given the complexity and polydispersity of these molecules. A fraction of this architecture may be present, but cannot be unambiguously detected by the techniques presented here.

It has been noted in literature that $T_{1\rho H}$ calculated using Eq. 1 or Eq. 2 is usually not very accurate,[68] which also explains the large errors associated some of the $T_{1\rho H}$ values in Tables 2 and 3. Unless observations are made up to very long contact times, where decay of the signal is clearly observable and substantial, the $T_{1\rho H}$ values are likely to be overestimated. However, comparisons can be made since all of them will be overestimated, the error being larger for larger values. As discussed in an earlier paper,[20] both highly mobile and rigid moieties have a long $T_{1\rho H}$, while anything in between have shorter values. The WY aliphatic groups generally appear to have longer values of $T_{1\rho H}$, ranging from 8.3 ± 5.9 to 19.8 ± 15.9 ms (ignoring the very long values which have errors larger than themselves), compared to those in UG8 ranging from 1.9 ± 0.1 to 5.5 ± 0.8 ms, which once again suggests that WY asphaltenes possess shorter alkyl sidechains. No significant differences in $T_{1\rho H}$ were observed between the aromatic carbons in UG8 and WY, which indicates similar sizes. The parameter b provides a measure of the dipolar coupling and is normally expected to be zero under magic angle spinning conditions. However, in Table 2 and 3 we see that most of the signals have non-zero b values, implying incomplete averaging of the $(3\cos^2\theta\text{-}1)$ term in the expression for b. The $(3\cos^2\theta\text{-}1)$ term describes the orientation dependence of the dipolar coupling

584 and chemical shift anisotropy (CSA), and incomplete averaging suggests that 8 kHz MAS is not
585 sufficient to fully average the CSA or the dipolar coupling. For CP purposes, this is important
586 since sufficient dipolar coupling is required for efficient transfer of magnetization, however, lower
587 speeds mean a greater effect of the CSA, in the form of sidebands overlapping the signals of
588 interest. Not surprisingly, the carbons with attached protons, and the rigid ones, show *b* values
589 larger (> 7.0 kHz) than those without protons and the mobile groups (< 1.0 kHz). This is due to
590 larger effective dipolar coupling, lending validation to the fitting calculations. Moreover, the
591 mobile –CH_3 groups (UG8: 22.71, 19.64, 14.03 ppm; WY: 22.88, 19.38, 14.36 ppm) show smaller
592 *b* values (< 1 kHz) compared to the other chain and cyclic alkyl groups. The *b* term quantifies the
593 rate of oscillatory exchange of magnetization between carbons and protons during CP,[69] which
594 scales with the size of the ^{1}H spin bath corresponding to the carbon of interest.

595

596 **4.3. *^{13}C Pre-CP Refocused DIVAM***

597 The pre-CP refocused DIVAM nutation curves for the most intense signals are shown in
598 Fig. 5. The more mobile groups show more pronounced oscillations in intensity, and usually have
599 a zero crossing at the smaller excitation angles. Recall that since the filtering is performed on the
600 ^{1}H nucleus, the nutation curves represent the mobilities of the protons from which the CP is
601 occurring. Before discussing subtle differences, comparing the nutation curves of the aromatic
602 groups at a glance reveals that in UG8 asphaltenes, the aromatic carbon signals nutate more
603 coherently than the same groups in WY asphaltenes (UG8: 138.02, 129.28, 123.78, 118.53 ppm,
604 WY: 138.31, 127.44, 122.52 ppm), where the nutation profiles are more disparate. It suggests that
605 most of the aromatic moieties in UG8 asphaltenes are in a similar domain of mobility, while in
606 WY asphaltenes some are more rigid than others. This difference in mobility can be explained in

two possible ways: i) that WY coal asphaltenes are composed of some very large and some much smaller PAHs, or ii) smaller PAHs are tethered to the larger PAHs like in an archipelago structure. The WY asphaltene carbons resonating 127.44 ppm, a large fraction of which are $C_{H,ar}$ groups, appear to have been polarized by the most mobile of all the aromatic protons, including the ones in UG8. As noted in an earlier section, these protonated carbons (~127 ppm) can belong to smaller aromatic rings connected to a larger PAH system via a single bond, and are easily distinguishable from protonated carbons in the larger PAH from their chemical shifts.[78,79] Naturally, the protons in these smaller rings can be expected to be more mobile than those in the larger PAH. These observations point towards the presence of archipelago-type motifs in WY coal asphaltenes, where the one large PAH is bound to a much smaller PAH via a single bond. Thus, although archipelago type in nature, these tethers cannot be called 'aliphatic linkages' as often shown in a lot of traditional archipelago models.[85,86] Rather, these can be viewed as a single core but with a discontinuity in the aromatic network, since the "linkage" is likely between two aromatic carbons. Moreover, Schuler *et al*.[50] have recently demonstrated this to be true for a different coal asphaltene. The UG8 petroleum asphaltenes do not appear to have these higher chemical shift $C_{H,ar}$ groups and majority of the protonated aromatic carbons (123.78 and 118.53 ppm) appear less mobile than those in WY asphaltenes. If the UG8 asphaltenes do possess the pendant aromatic groups, their mobility is likely reduced due to the UG8 clusters being more closely packed than those in WY asphaltenes. The closer packing of the UG8 clusters is likely a result of the longer aliphatic chains that intercalate between the aromatic sheets,[20] which is discussed again below. Thus, although the presence of these pendant aromatics in UG8 cannot be ruled out, no evidence for their presence is observed here.

Among the C_{db} and C_{sub}-R groups (UG8: 138.02 ppm, WY: 138.31 ppm), those in UG8 show more pronounced oscillations and undergo a zero-crossing, while those in WY oscillate to a lesser extent and do not cross zero. This is a direct consequence of UG8 PA possessing longer alkyl sidechains. It provides a comparatively more mobile ^{1}H spin-bath to these carbons in UG8, as manifested in the DIVAM nutation profile, than the ones in WY, whose main spin-bath for CP are the rigid aromatic protons and short, rigid alkyl chains.

Among the aliphatic signals, the chain $–CH_2$ groups in UG8, especially those not directly attached to aryl rings (22.71, 29.77 ppm), show a greater degree of mobility compared to those in WY (22.88, 29.82 ppm), as shown by the former's more pronounced nutation profiles. The branched and aryl $–CH_3$ groups in UG8 (19.64 ppm) also show greater mobility than the same groups in WY (19.38 ppm). These observations are consistent with UG8 PA possessing longer, hence more mobile aliphatic sidechains. The terminal $–CH_3$ groups in WY (14.36 ppm) show more pronounced oscillations than those in UG8 (14.30 ppm), indicating greater mobility, but its behavior is somewhat erratic at smaller excitation angles. This could simply be an effect of one of the spinning sidebands of the 138.31 ppm signal (see Fig. 1) having significant overlap with the 14.36 ppm signal, which adds error to the observed intensity. This issue can likely be avoided if the experiment is performed at a lower magnetic field if available, since the sideband intensity would be proportionately less and the aromatic sidebands will be displace beyond the aliphatic region. Nonetheless, at larger angles the sideband gets filtered out and the nutation behavior returns to normal. The UG8 terminal methyl groups, interestingly, also appear less mobile than the chain methylene groups. This is only possible when the motion of the methyl groups are restricted by interaction with other groups. It was hypothesized previously in this paper that alkyl chains can intercalate between the stacked aromatic cores of an aggregate, which would also hinder the

motion of terminal groups. Thus, the reduced mobility of terminal –CH_3 groups in UG8 PA corroborate this hypothesis. This is not the case for WY CDA, where the alkyl chains are too short have any such interaction. In a previous paper,[20] we provided evidence for the same intercalation behaviour in bitumen derived asphaltenes, which appear to be structurally similar to PA. These aliphatic-aromatic interactions likely result in more closely packed clusters in UG8 PA, and may have important implications in determining the role of the alkyl sidechains in the aggregation of asphaltenes, but it can only be addressed conclusively by observing asphaltene behavior in a range of concentrations in the solution-state, which shall be investigated in a separate study.

The 29.59 ppm UG8 signal shows reduced mobility, justifying its assignment to alicyclic carbons. All the other aliphatic carbons in both asphaltenes show reduced mobility, as expected from groups attached to the aromatic core.

4.4. *Optical Spectra*

Figure 6 shows the optical spectra of UG8 and WY asphaltenes. Because optical absorption occurs in aromatic carbons, the spectra are normalized to the amount of aromatic carbon, which is larger in WY asphaltenes compared the UG8 asphaltenes. Absorption at larger wavelengths indicates the presence of ring systems that are larger and/or contain more isolated double bonds as opposed to aromatic sextets in the Clar representation of PAHs.[87] Wide variation in the absolute absorption but similar spectral shapes have been noted previously for different crude oils, indicating a large difference in the concentration of optical absorbers (primarily the asphaltenes) but a general similarity in the composition of the PAH distributions.[88] Here the spectra of both asphaltenes are relatively similar, indicating PA and CDA have similar aromatic cores, consistent

674 with the NMR spectroscopy results. Spectra in this range (250 –3,300 nm) typically are more
675 sensitive to the dominant ring systems in asphaltenes.[7,8] Despite the overall similarity, there is a
676 subtle difference in which the spectrum of CDA shows a steeper slope than the spectrum of PA at
677 lower wavelength, while the spectra converge at higher wavelength. The similarity at high
678 wavelength suggest the largest ring systems in CDA and PA are relatively similar, while the steeper
679 slope for CDA at low wavelength suggests somewhat greater abundance of smaller ring systems
680 in the CDA, confirming the observation made earlier using NMR spectroscopy. Overall, the optical
681 spectra are consistent with similar but not identical PAH distributions PAs vs CDAs. Moreover,
682 different studies find somewhat different results on the extent of similarity of PAHs for PAs and
683 CDAs, which could be due to different sensitivities of various techniques to specific PAH ring
684 sizes.

685

686 **5. Conclusions**

687 Using solid-state NMR spectroscopic techniques to compare petroleum and coal derived
688 asphaltenes, we demonstrate how CP dynamics and quantitative DP ^{13}C NMR experiments can be
689 used in a complementary fashion. Neither CP nor the DP experiment by itself appear to be
690 sufficient in providing a complete description of the asphaltene molecules. While DP provides an
691 overall quantitative description, CP methods are more sensitive to the smaller PAH systems. The
692 refocused DIVAM experiment offers a novel way to investigate the molecular dynamics of the
693 complex asphaltenes and demonstrates how solid-state NMR pulse sequences originally developed
694 for polymer characterization can also be used to study naturally occurring organic matter. Using
695 the above techniques, key structural differences between the two asphaltenes, UG8 and WY,
696 derived from petroleum and coal respectively, were identified, and insights were gained into the

697 distribution of PAH sizes. It was shown that the asphaltene molecular architecture consists of a
698 spectrum of sizes, ranging from smaller PAHs (<5 condensed rings) to much larger ones (>9
699 condensed rings), but their distribution varies between the two asphaltenes studied here. The
700 preponderance of the bridgehead carbon fraction in both asphaltenes shows that the dominant
701 architecture constitutes the larger pericondensed PAHs. The CP dynamics, quantitative NMR and
702 optical spectroscopy results all show that WY asphaltenes have a greater of abundance of the
703 smaller PAHs, while the larger PAHs are similar in size for both asphaltenes. The similarity of the
704 largest cores on P and CD asphaltenes is further reinforced by the optical spectra. The CP refocused
705 DIVAM results suggest that WY CDA may have archipelago-type structures, where a small PAH
706 is tethered to the larger PAH core via a single bond between aromatic carbons. This is also
707 consistent with the WY CDA having a greater fraction of smaller PAHs. The lack of any traditional
708 archipelago structures in asphaltenes (with separate PAHs linked by alkane groups) has recently
709 been determined by direct molecular imaging;[50] all NMR results herein were also unable to detect
710 any traditional archipelago structures for both petroleum asphaltenes and coal derived asphaltenes.
711 For example, the mobilities of different aromatic carbon in PAs are shown to be fairly similar, thus
712 it is not expected to have pendant benzene rings attached tethered by (mobile) alkane linkages.
713 Thus, a single core model still dominates. Nevertheless, further investigation of this molecular
714 structural issue is desirable, provided the complexity of the molecules, and traditional archipelago
715 structures cannot be completely ruled out. The UG8 PA have longer alkyl chains and a larger
716 fraction of alicyclic groups. On account of the longer length, with an average of ~7 carbons, the
717 alkyl chains in UG8 intercalate between the aromatic rings of adjacent asphaltene aggregates. This
718 is not observed in WY asphaltenes, because of shorter alkyl chains which are ~3-4 carbons long
719 on average. This is a major distinction between PA and CDA and may have important implications

on the role of alkyl sidechains in asphaltene aggregation. UG8 asphaltenes also have a greater number of sulfur containing groups, which are absent, or present in insignificant amounts in WY asphaltenes. To understand how these structural differences manifest in asphaltene aggregation behavior, solution-state NMR studies at various asphaltene concentrations are required.

Table 1. Description of the different carbon types numbered in Figure 2.

Carbon # in Figure 2	Type of carbon	Carbon # in Figure 2	Type of carbon
1	C_{sub}-O-C[a]	11	'bay' type $C_{H,ar}$[a]
2	C_{sub}-N[a]	12	CH_3-aryl
3	$C_{H,ar}$ 'α' to C_{sub}-N[a]	13	'fjord' type $C_{H,ar}$[a]
4	Cyclic *C*H	14	Acyclic aliphatic -*C*H
5	$-CH_2$-S-R/cyclic $-CH_2$	15	isobutyl $-CH_3$
6	C_{sub}-O-H[a]	16	C_{sub}-R[a]
7	$C_{H,ar}$ 'α' to C_{sub}-O[a]	17	$C_{H,ar}$-S-R
8	branched $-CH_3$	18	C_{db}[a]
9	ali. [a] $-CH_2$ not 'α' to ar. or to term. Methyl group	19	C_{tb}[a]
10	terminal $-CH_3$	20	$C_{H,ar}$ on pendant aromatic ring

[a]$C_{H,ar}$ = aromatic –CH; C_{sub} = substituted/ipso aromatic C; C_{db} = double bridgehead aromatic C; C_{tb} = triple bridgehead aromatic C. ali. = aliphatic.

Table 2. CP dynamics parameters for the deconvolved ^{13}C CP-MAS peaks of UG8 PA

UG8 Petroleum Asphaltenes						
$\delta\{^{13}C\}$ ppm	Assignment	T_{CP1}, ms (R_1, kHz)	T_{CP2}, ms (R_2, kHz)	$T_{1\rho H}$, ms	$b/2\pi$, kHz	%C
162.51	C_{sub}-O-C/ C_{sub}-O-H	0.05±0.02 (20.0±8.0)	1.96±0.73 (0.5±0.2)	14.4 ±10.9	0.5 ±0.2	2.0 ±0.7
147.51	C_{sub}-N	0.03±0.03 (33.3±33.3)	0.77±0.21 (12.9±3.4)	25.1 ±21.8	0.6 ±0.2	3.5 ±0.1
138.02	C_{sub}-R/C_{db}	0.25±0.05 (4.0±0.8)	1.89±0.39 (0.5±0.1)	13.3 ±2.5	0.5±0.2	13.3 ±0.6
129.28	C_{db}/C_{tb}	0.12±0.01 (8.3±0.7)	2.71±0.28 (1.0±0.1)	10.6 ±1.7	0.5 ±0.0	16.3 ±6.5
123.78	$C_{H,ar}$/ $C_{H,ar}$-S-R	0.05±0.01 (20.0±4.0)	0.07±0.01 (14.3±2.0)	5.28 ±0.48	9.5 ±1.6	5.9 ±0.5
118.53	$C_{H,ar}$: 'bay' type and 'α' to C_{sub}-O/N	0.06±0.02 (16.7±5.6)	0.05±0.01 (20.0±4.0)	10.9 ±2.4	15.9 ±4.8	5.5 ±0.2
109.58	$C_{H,ar}$	0.19±0.08 (5.3±2.2)	0.06± 0.02 (16.7±5.6)	5.8 ±2.0	11.1 ±1.6	2.3 ±0.1
44.03	ali. or cyc. *C*-S-R/cyclic -*C*H	0.12±0.02 (8.3±1.4)	0.05±0.01 (20.0±4.0)	5.5 ±0.8	11.1 ±1.6	5.1 ±0.2
37.45	cyclic -*C*H.	0.05±0.01 (20.0±4.0)	0.05±0.01 (20.0±4.0)	5.3 ±0.2	15.9 ±1.6	5.6 ±0.1
31.98	ali. –*CH*, -ali./cyc -CH_2 'α' to ar.	0.05±0.01 (20.0±4.0)	0.15±0.03 (6.7±1.3)	1.9 ±0.1	19.1 ±0.3	1.8 ±0.0
29.77	ali. –CH_2 not 'α' to ar. or to term. meth.	0.21±0.00 (4.8±0.1)	0.08±0.04 (12.5±6.3)	2.9 ±0.3	-4.8±0.9	9.7 ±3.1
29.59	ali. –CH_2/cyc. –CH_2/cyc. –CH_2-S-R	0.07±0.01 (14.3±2.0)	0.05±0.01 (20.0±4.0)	3.0 ±0.1	7.9 ±1.6	22.6 ±0.0
22.71	isobut. –CH_3/-CH_2 'α' to term. meth.	0.09±0.02 (11.1±2.5)	1.24±0.77 (0.8±0.5)	2.6 ±0.5	0.3±0.2	2.2 ±0.1
19.64	CH_3-ar./branched –CH_3	0.07±0.01 (14.3±1.0)	0.67±0.16 (1.5±0.4)	3.3 ±0.3	-0.3±0.2	4.4 ±0.1
14.30	term.-CH_3	0.11±0.02 (9.1±1.7)	0.71±0.69 (1.4±1.4)	4.8 ±2.0	0.5±0.3	3.0 ±0.7

T_{CP1} and T_{CP2} are the CP time constants. R_1 and R_2 are the CP rate constants.$T_{1\rho H}$ is the longitudinal relaxation in the rotating frame. The quantity b is the C-H dipolar coupling constant. The b obtained from the fitting was in radians/s, hence was divided by 2π to obtain the kHz value. The %C values were calculated using Eq. 3. $C_{H,ar}$ = aromatic –CH; C_{sub} = substituted/ipso aromatic C; C_{db} = double bridgehead aromatic C; C_{tb} = triple bridgehead aromatic C. ali. = aliphatic; isobut. = isobutyl; meth = methyl; term. = terminal. The assigned carbon types are described in Fig. 2 and Table 1.

Table 3. CP dynamics parameters for the deconvolved ^{13}C CP-MAS peaks of Wyoming CDA.

Wyoming (WY) Coal Derived Asphaltenes						
$\delta\{^{13}C\}$ ppm	Assignment	T_{CP1}, ms (R_1, kHz)	T_{CP2}, ms (R_2, kHz)	$T_{1\rho H}$, ms	$b/2\pi$, kHz	%C
155.54	C_{sub}-O-H/ C_{sub}-N	0.05±0.01 (20.0±4.0)	1.99±0.28 (0.5±0.1)	18.2 ±6.3	0.6±0.1	7.5 ±0.2
138.31	C_{sub}-R/C_{db}	0.22±0.04 (4.5±0.8)	2.81±0.56 (0.3±0.1)	13.1 ±3.0	0.5±0.1	25.1 ±1.6
127.44	C_{tb} / $C_{H,ar}$ of small pendant rings	0.04±0.01 (25.0±6.3)	4.13±1.2 (0.2±0.1)	5.2 ±0.9	0.5±0.1	28.8 ±1.2
122.52	C_{tb}/'bay' type $C_{H,ar}$	0.07±0.01 (14.3±2.0)	0.05±0.01 (20.0±4.0)	17.8 ±4.1	9.5±2.2	11.7 ±0.3
111.59	$C_{H,ar}$	0.11±0.04 (9.1±3.3)	0.09±0.08 (11.1±9.9)	5.3±1.7	17.5 ±3.2	6.0 ±0.6
38.78	cyclic -CH.	0.19±0.05 (5.3±1.4)	0.13±0.06 (7.7±3.6)	19.8±15.9	15.9 ±0.6	5.6 ±0.9
31.96	ali. –CH, -ali./cyc -CH_2 'α' to ar.	0.06±0.03 (16.7±8.4)	0.26±0.09 (3.8±2.9)	40.9±103.5	15.9 ±0.8	2.7 ±0.2
29.82	ali. –CH_2 not 'α' to Ar. or term. meth	0.09±0.06 (11.1±7.4)	0.04±0.02 (25.0±12.5)	10.6±6.3	0	4.7 ±0.3
22.88	isobut. –CH_3/-CH_2 'α' to term. meth.	0.04±0.01 (25.0±6.3)	0.35±0.08 (2.9±0.7)	10.9±6.0	0	3.0 ±0.2
19.38	CH_3-Ar./branched –CH_3	0.04±0.01 (25.0±6.3)	0.57±0.09 (1.8±0.2)	93.5±149.4	0.9±0.9	2.1 ±0.1
14.36	term.-CH_3	0.04±0.01 (25.0±6.3)	2.11±1.02 (0.5±0.2)	8.3±5.9	0.6±0.6	2.9 ±0.1

T_{CP1} and T_{CP2} are the CP time constants. R_1 and R_2 are the CP rate constants. $T_{1\rho H}$ is the longitudinal relaxation in the rotating frame. The quantity b is the C-H dipolar coupling constant. The b obtained from the fitting was in radians/s, hence was divided by 2π to obtain the kHz value. The %C values were calculated using Eq. 3. $C_{H,ar}$ = aromatic –CH; C_{sub} = substituted/ipso aromatic C; C_{db} = double bridgehead aromatic C; C_{tb} = triple bridgehead aromatic C. ali. = aliphatic; isobut. = isobutyl; meth = methyl; term. = terminal. The assigned carbon types are described in Fig. 2 and Table 1.

774 **Table 4.** Structural parameters for UG8 and WY asphaltenes calculated from the %*C* values
775 obtained from Eq. 3 (CP) and from the DP ^{13}C spectra.

	UG8		WY	
Structural Parameters	CP	DP*	CP	DP*
aromaticity	47.2 ± 2.4%	64.2 ± 0.5%	81.2 ± 2.3%	82.1 ± 0.1%
aliphaticity	52.8 ± 6.5%	35.8 ± 0.3%	18.8 ± 5.5%	17.9 ± 0.0%
$C_{H,ar}$[a]	13.3 ± 6.4 %	13.4 ± 0.2%	17.8 ± 2.6%	10.1 ± 0.0%
C_{sub}[a]	15.5 ± 7.9 %	17.0 ± 0.6%	28.1 ± 1.7%	25.7 ± 0.0%
$C_{sub,ali}$[a]	10.2 ± 3.9%	14.6 ± 0.2%	20.7 ± 5.1%	20.9 ± 0.0%
$C_{db} + C_{tb}$[a]	18.5 ± 3.6%	33.8 ± 0.3%	35.3 ± 3.9%	46.3 ± 0.1%
aromatic condensation index (χ_b) [a]	0.40 ± 0.02	0.53 ± 0.30	0.40 ± 0.02	0.56 ± 0.06
rings in a single core	5 to 6	>7	5 to 6	>9
average alkyl chain length	10.7	5.5	4.9	2.7
alkyl carbons α to sulfur groups	5.1 ± 3.4%	3.5 ± 0.1%	negligible	negligible

776 [a]$C_{H,ar}$ = aromatic –CH, including heteroaromatics; $C_{sub,}$ = substituted/ipso aromatic C; $C_{sub,ali}$ = alkyl substituted/ipso
777 aromatic C; C_{db} = double bridgehead aromatic C; C_{tb} = triple bridgehead aromatic C. *Relative errors for the
778 parameters from DP spectra were calculated with a 3σ corresponding to 99.7% confidence level, obtained from the
779 residual error (χ2) in the deconvolution analysis. The errors in the CP based calculations are associated with the
780 errors in the fitting of Eq. 3 with the variable contact time data.
781
782
783
784
785
786
787

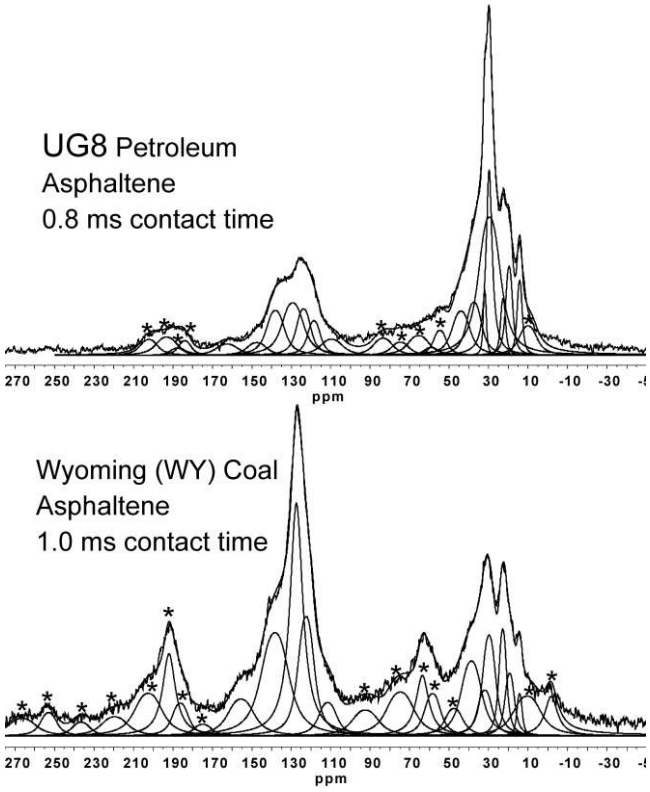

788

789 **Figure 1.** ^{13}C CP-MAS NMR spectra of (top) UG8 petroleum asphaltenes and (bottom) Wyoming
790 coal asphaltenes obtained under 8 kHz MAS, with 0.8 and 1.0 ms contact times respectively,
791 showing the deconvolved peaks. Asterisks (*) denote the spinning sidebands. For the DP-MAS
792 spectra, see Supporting Information.

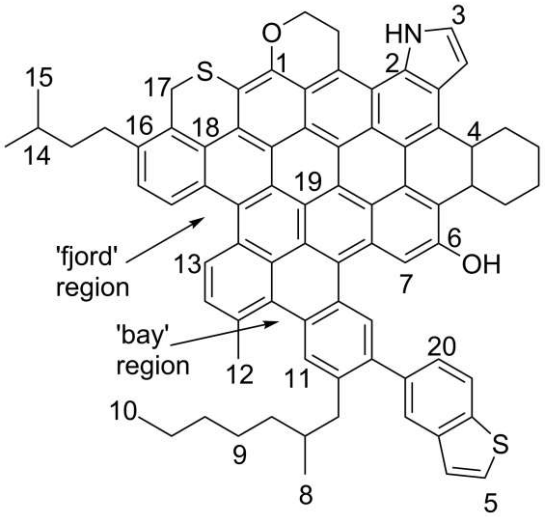

793

794 **Figure 2.** Hypothetical asphaltene molecule showing the different carbon types for which were
795 assigned to the fitted peaks in the CP-MAS spectra. The types of carbons corresponding to each
796 number on the figure are listed in Table 1.
797

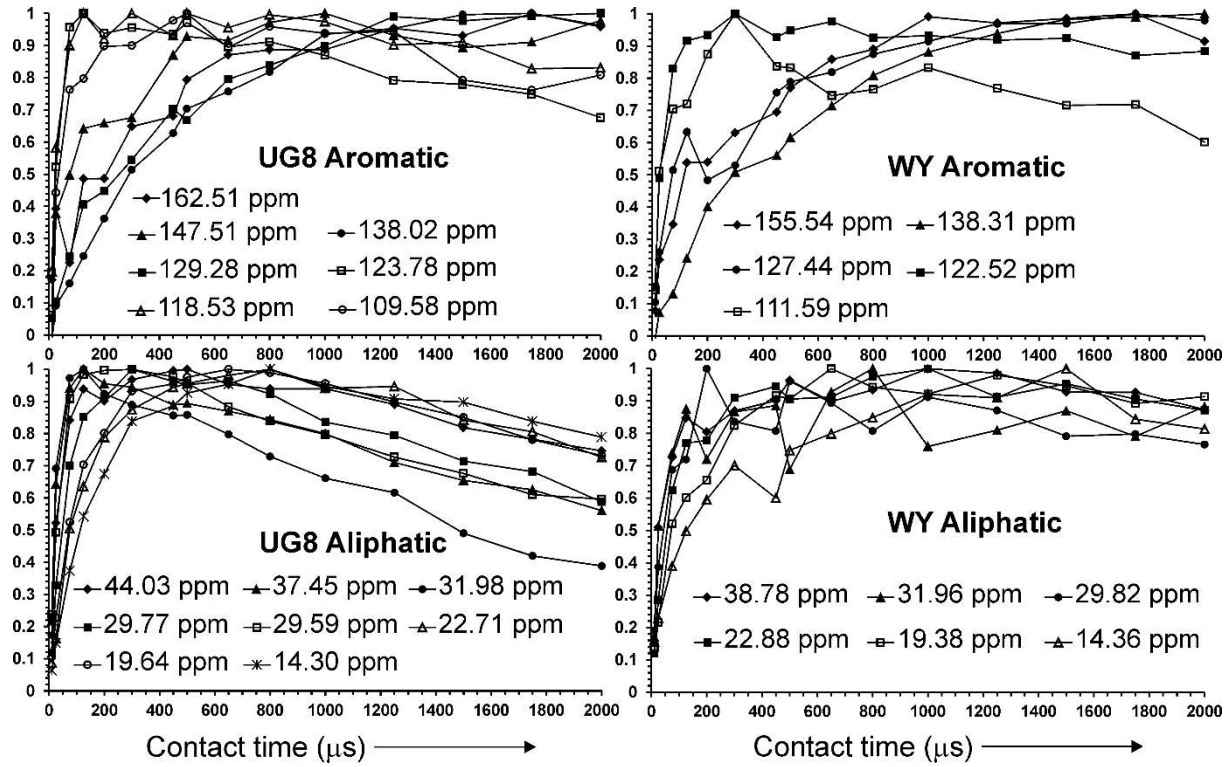

Figure 3. ^{1}H-to-^{13}C cross-polarization build-up curves for the deconvolved peaks of the ^{13}C CP-MAS NMR spectra of UG8 and WY asphaltenes. The normalized intensities are plotted against increasing contact time. The faster decay of the UG8 aliphatic signals at longer contact times (i.e. shorter $T_{1\rho H}$) suggests greater mobility, consistent with longer sidechains in PA.

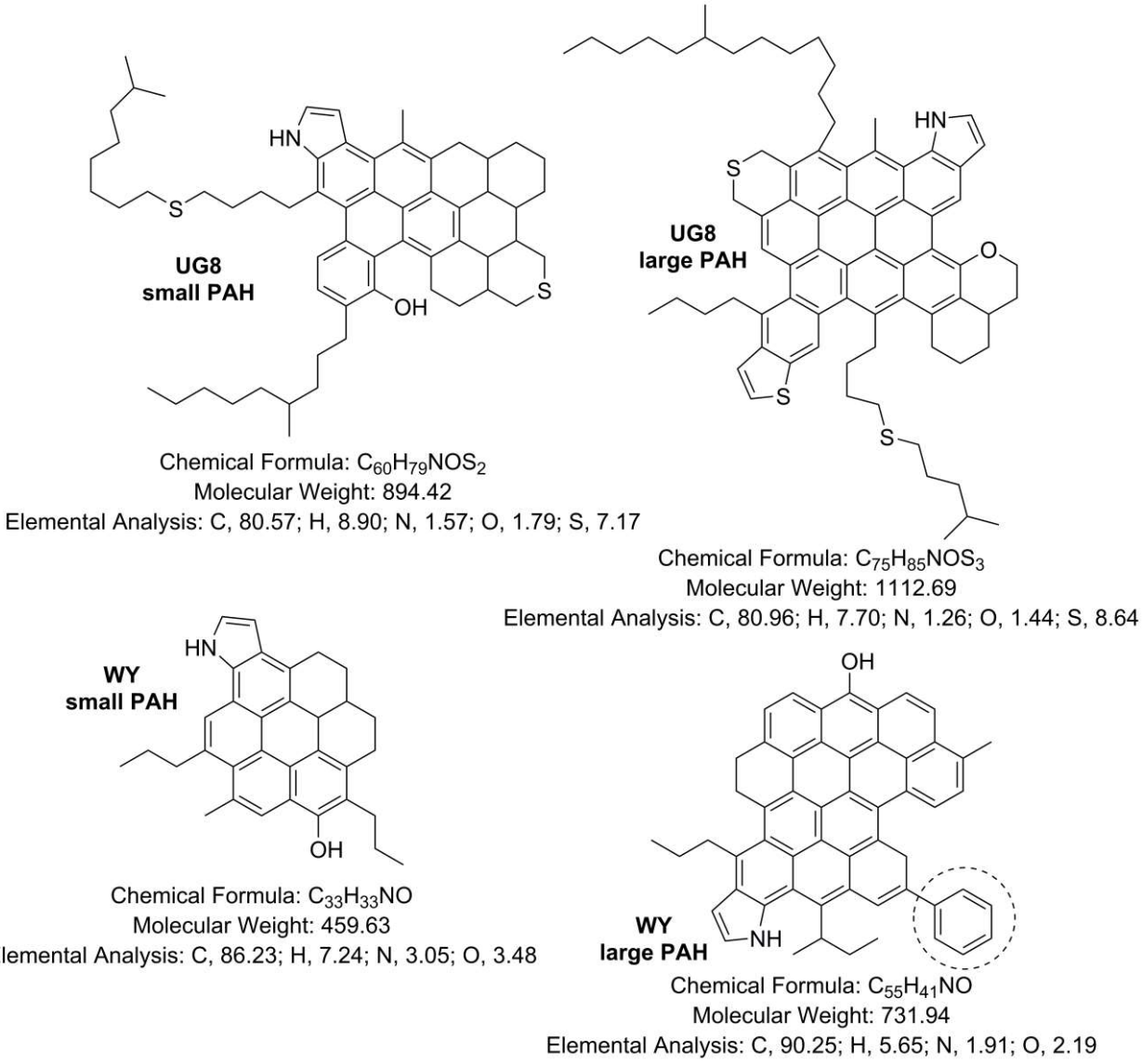

804

805 **Figure 4.** Average hypothetical structures of UG8 PA and WY CDA based on the calculated
806 parameters, elemental analysis and H:C ratios. Two different PAH sizes, large and small, have
807 been shown for each to represent the calculated limits. The dashed circle highlights the pendant
808 aromatic ring, corresponding to "archipelago type" structures. The sulfur moieties (sulfide and
809 thiophene) were chosen based on the most abundant sulfur groups in Kuwaiti oils.[89]

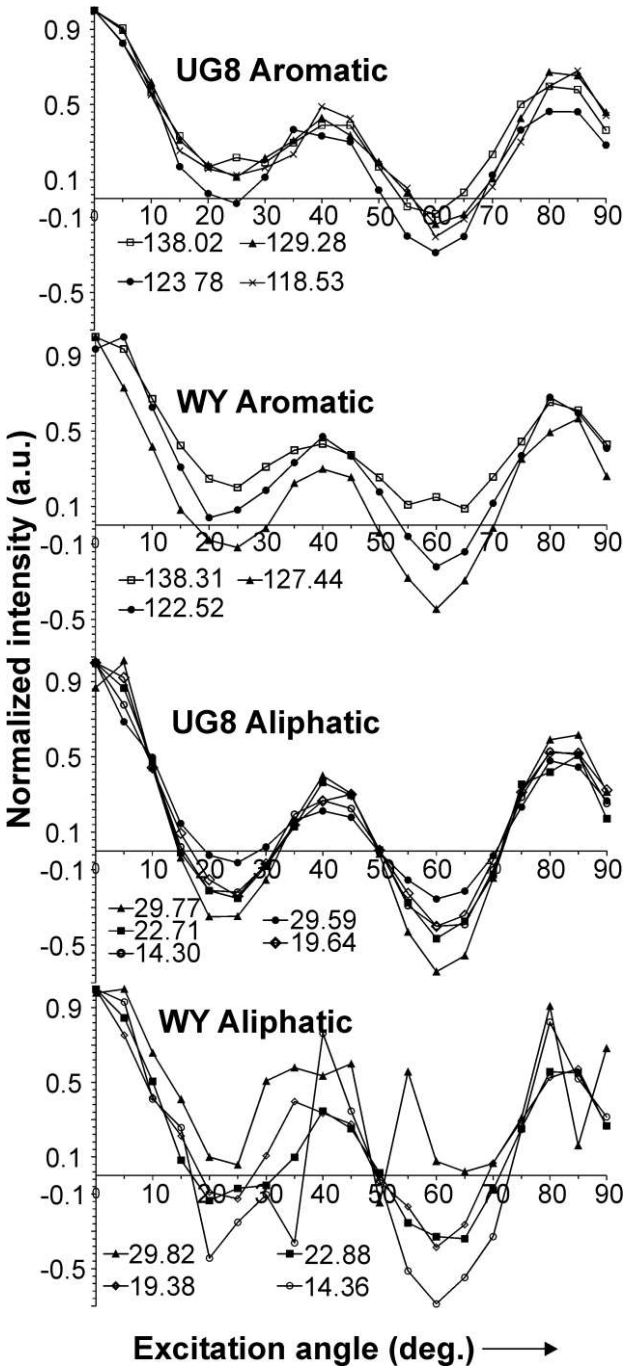

Figure 5. Pre-CP refocused DIVAM nutation curves for the deconvolved peaks of the ^{13}C CP-MAS NMR spectra of UG8 and WY asphaltenes. The nutation curves for only the most intense signals are shown. The aromatic nutation curves (top two) show that there is more variability in the nutation behavior of the WY CDA compared to UG8 PA, likely due to a greater abundance of smaller ring systems and/or archipelago-type structures.

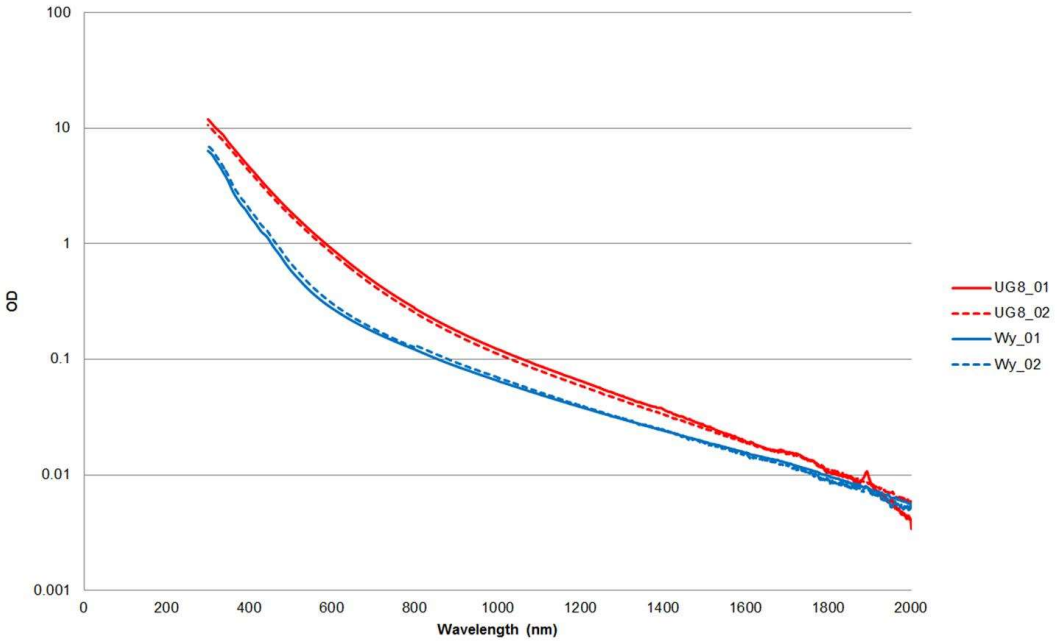

Figure 6. Optical spectra of UG8 (PA) and Wy (CDA). Each asphaltene sample was scanned twice (scan numbers 01 and 02) and shows good reproducibility. The similarity of the slopes at high wavelength suggest that the largest ring systems in CDA and PA are relatively similar, while the steeper slope for CDA at low wavelength suggests somewhat greater abundance of smaller ring systems in the CDA.

Notes

The authors declare no competing financial interest.

Acknowledgments

M.G. and P.H. thank the Natural Sciences and Engineering Research Council of Canada (NSERC) for financial support. We thank Tony Montina, University of Lethbridge NMR manager and Michael Opyr for their help with setting up the refocused DIVAM experiment.

References

(1) Mullins, O. C. *Energy Fuels* **2010**, *24*, 2179-2207.

(2) Mullins, O. C.; Sabbah, H.; Eyssautier, J.; Pomerantz, A. E.; Barré, L.; Andrews, A. B.; Ruiz-Morales, Y.; Mostowfi, F.; McFarlane, R.; Goual, L.; Lepkowicz, R.; Cooper, T.; Orbulescu, J.; Leblanc, R. M.; Edwards, J.; Zare, R. N. *Energy Fuels* **2012**, *26*, 3986-4003.

(3) Groenzin, H.; Mullins, O. C. *J. Phys. Chem. A* **1999**, *103*, 11237-11245.

(4) Groenzin, H.; Mullins, O. C. *Energy Fuels* **2000**, *14*, 677-684.

(5) Guerra, R. E.; Ladavac, K.; Andrews, A. B.; Mullins, O. C.; Sen, P. N. *Fuel* **2007**, *86*, 2016-2020.

(6) Lisitza, N. V; Freed, D. E.; Sen, P. N.; Song, Y.-Q. *Energy Fuels* **2009**, *23*, 1189-1193.

(7) Ruiz-Morales, Y.; Wu, X.; Mullins, O. C. *Energy Fuels* **2007**, *21*, 944-952.

(8) Ruiz-Morales, Y.; Mullins, O. C. *Energy Fuels* **2009**, *23*, 1169-1177.

(9) Andreatta, G.; Bostrom, N.; Mullins, O. C. *Langmuir* **2005**, *21*, 2728-2736.

(10) Hortal, A. R.; Hurtado, P.; Martínez-Haya, B.; Mullins, O. C. *Energy Fuels* **2007**, *21*, 2863-2868.

(11) Rodgers, R. P.; Marshall, A. G. In *Asphaltenes, Heavy Oils and Petroleomics*; Mullins, O. C.; Sheu, E. Y.; Hammami, A.; Marshall, A. G., Eds.; Springer: New York, 2007; pp. 63–93.

(12) Zeng, H.; Song, Y.-Q.; Johnson, D. L.; Mullins, O. C. *Energy Fuels* **2009**, *23*, 1201-1208.

(13) Goual, L.; Sedghi, M.; Zeng, H.; Mostowfi, F.; McFarlane, R.; Mullins, O. C. *Fuel* **2011**, *90*, 2480-2490.

(14) Indo, K.; Ratulowski, J.; Dindoruk, B.; Gao, J.; Zuo, J.; Mullins, O. C. *Energy Fuels* **2009**, *23*, 4460-4469.

(15) Mostowfi, F.; Indo, K.; Mullins, O. C.; McFarlane, R. *Energy Fuels* **2008**, *23*, 1194-1200.

(16) Barré, L.; Jestin, J.; Morisset, A.; Palermo, T.; Simon, S. *Oil Gas Sci. Technol. - Rev. IFP* **2009**, *64*, 617-628.

(17) Eyssautier, J.; Levitz, P.; Espinat, D.; Jestin, J.; Gummel, J.; Grillo, I.; Barré, L. *J. Phys. Chem. B* **2011**, *115*, 6827-6837.

(18) Anisimov, M. A.; Yudin, I. K.; Nikitin, V.; Nikolaenko, G.; Chernoutsan, A.; Toulhoat, H.; Frot, D.; Briolant, Y. *J. Phys. Chem.* **1995**, *99*, 9576-9580.

(19) Dutta Majumdar, R.; Gerken, M.; Mikula, R.; Hazendonk, P. *Energy Fuels* **2013**, *27*, 6528-6537.

(20) Dutta Majumdar, R.; Gerken, M.; Hazendonk, P. *Energy Fuels* **2015**, *29*, 2790-2800.

(21) Andrews, A. B.; Edwards, J. C.; Pomerantz, A. E.; Mullins, O. C.; Nordlund, D.; Norinaga, K. *Energy Fuels* **2011**, *25*, 3068-3076.

(22) Korb, J.-P.; Louis-Joseph, A.; Benamsili, L. *J. Phys. Chem. B* **2013**, *117*, 7002-7014.

(23) Sabbah, H.; Morrow, A. L.; Pomerantz, A. E.; Zare, R. N. *Energy Fuels* **2011**, *25*, 1597-1604.

(24) Pomerantz, A. E.; Wu, Q.; Mullins, O. C.; Zare, R. N. *Energy Fuels* **2015**, *29*, 2833-2842.

(25) Wu, Q.; Pomerantz, A. E.; Mullins, O. C.; Zare, R. N. *Energy Fuels* **2014**, *28*, 475-482.

(26) Pinkston, D. S.; Duan, P.; Gallardo, V. A.; Habicht, S. C.; Tan, X.; Qian, K.; Gray, M.; Müllen, K.; Kenttämaa, H. I. *Energy Fuels* **2009**, *23*, 5564-5570.

(27) Rane, J. P.; Harbottle, D.; Pauchard, V.; Couzis, A.; Banerjee, S. *Langmuir* **2012**, *28*, 9986-9995.

(28) Rane, J. P.; Pauchard, V.; Couzis, A.; Banerjee, S. *Langmuir* **2013**, *29*, 4750-4759.

(29) Pauchard, V.; Rane, J. P.; Zarkar, S.; Couzis, A.; Banerjee, S. *Langmuir* **2014**, *30*, 8381-8390.

(30) Badre, S.; Carla Goncalves, C.; Norinaga, K.; Gustavson, G.; Mullins, O. C. *Fuel* **2006**, *85*, 1-11.

(31) Buch, L.; Groenzin, H.; Buenrostro-Gonzalez, E.; Andersen, S. I.; Lira-Galeana, C.; Mullins, O. C. *Fuel* **2003**, *82*, 1075-1084.

(32) Wargadalam, V. J.; Norinaga, K.; Iino, M. *Fuel* **2002**, *81*, 1403-1407.

(33) Rane, J. P.; Zarkar, S.; Pauchard, V.; Mullins, O. C.; Christie, D.; Andrews, A. B.; Pomerantz, A. E.; Banerjee, S. *Energy Fuels* **2015**, *29*, 3584-3590.

(34) Hurt, M. R.; Borton, D. J.; Choi, H. J.; Kenttämaa, H. I. *Energy Fuels* **2013**, *27*, 3653-3658.

(35) Freed, D. E.; Mullins, O. C.; Zuo, J. Y. *Energy Fuels* **2010**, *24*, 3942-3949.

(36) Zuo, J. Y.; Mullins, O. C.; Freed, D.; Elshahawi, H.; Dong, C.; Seifert, D. J. *Energy Fuels* **2013**, *27*, 1722-1735.

(37) Mullins, O. C.; Pomerantz, A. E.; Andrews, A. B.; Zuo, J. Y. *Petrophysics*, **2015**, *56*, 266–275.

(38) Mullins, O. C.; Seifert, D. J.; Zuo, J. Y.; Zeybek, M. *Energy Fuels* **2013**, *27*, 1752-1761.

(39) Mullins, O. C.; Betancourt, S. S.; Cribbs, M. E.; Dubost, F. X.; Creek, J. L.; Andrews, A. B.; Venkataramanan, L. *Energy Fuels* **2007**, *21*, 2785-2794.

(40) Betancourt, S. S.; Ventura, G. T.; Pomerantz, A. E.; Viloria, O.; Dubost, F. X.; Zuo, J.; Monson, G.; Bustamante, D.; Purcell, J. M.; Nelson, R. K.; Rodgers, R. P.; Reddy, C. M.; Marshall, A. G.; Mullins, O. C. *Energy Fuels* **2009**, *23*, 1178-1188.

(41) Achourov, V.; Pfeiffer, T.; Kollien, T.; Betancourt, S. S.; Zuo, J. Y.; di Primio, R.; Mullins, O. C. *Petrophysics* **2015**, *56*, 346-357.

(42) Forsythe, J. C.; Pomerantz, A. E.; Seifert, D. J.; Wang, K.; Chen, Y.; Zuo, J. Y.; Nelson, R. K.; Reddy, C. M.; Schimmelmann, A.; Sauer, P.; Peters, K. E.; Mullins, O. C. *Energy Fuels* **2015**, *29*, 5666-5680.

(43) Zuo, J. Y.; Pan, S.; Chen, C.; Wang, K.; Mullins, O. C. Modelling of Density Inversion from Gas Charges into Oil Reservoirs Using Diffusion and Flory-Huggins-Zuo Equations

Ind. Eng. Chem. Res., submitted for publication, 2015.

(44) Zuo, J. Y.; Jackson, R.; Agarwal, A.; Herold, B.; Kumar, S.; Santo, I. De; Dumont, H.; Ayan, C.; Beardsell, M.; Mullins, O. C. *Energy Fuels* **2015**, *29*, 1447-1460.

(45) Andrews, A. B.; McClelland, A.; Korkeila, O.; Demidov, A.; Krummel, A.; Mullins, O. C.; Chen, Z. *Langmuir* **2011**, *27*, 6049-6058.

(46) Yang, F.; Tchoukov, P.; Pensini, E.; Dabros, T.; Czarnecki, J.; Masliyah, J.; Xu, Z. *Energy Fuels* **2014**, *28*, 6897-6904.

(47) Tang, W.; Hurt, M. R.; Sheng, H.; Riedeman, J. S.; Borton, D. J.; Slater, P.; Kenttämaa, H. I. *Energy Fuels* **2015**, *29*, 1309-1314.

(48) Karimi, A.; Qian, K.; Olmstead, W. N.; Freund, H.; Yung, C.; Gray, M. R. *Energy Fuels* **2011**, *25*, 3581-3589.

(49) Alshareef, A. H.; Scherer, A.; Tan, X.; Azyat, K.; Stryker, J. M.; Tykwinski, R. R.; Gray, M. R. *Energy Fuels* **2011**, *25*, 2130-2136.

(50) Schuler, B.; Meyer, G.; Peña, D.; Mullins, O. C.; Gross, L. *J. Am. Chem. Soc.* **2015**, *137*, 9870-9876.

(51) Cyr, N.; McIntyre, D. D.; Toth, G.; Strausz, O. P. *Fuel* **1987**, *66*, 1709-1714.

(52) Storm, D. A.; Edwards, J. C.; DeCanio, S. J.; Sheu, E. Y. *Energy Fuels* **1994**, *8*, 561-566.

(53) Christopher, J.; Sarpal, A. S.; Kapur, G. S.; Krishna, A.; Tyagi, B. R.; Jain, M. C.; Jain, S. K.; Bhatnagar, A. K. *Fuel* **1996**, *75*, 999-1008.

(54) Fossen, M.; Kallevik, H.; Knudsen, K. D.; Sjöblom, J. *Energy Fuels* **2011**, 3552-3567.

(55) Weinberg, V. A.; Yen, T. F.; Murphy, P. D.; Gerstein, B. C. *Carbon* **1983**, *21*, 149-156.

(56) Weinberg, V. L.; Yen, T. F.; Gerstein, B. C.; Murphy, P. D. *Prepr. - Am. Chem. Soc., Div. Pet. Chem.* **1981**, *26*, 816-824.

(57) Murphy, P. D.; Gerstein, B. C.; Weinberg, V. L.; Yen, T. F. *Anal. Chem.* **1982**, *54*, 522-525.

(58) Semple, K. M.; Cyr, N.; Fedorak, P. M.; Westlake, D. W. S. *Can. J. Chem.* **1990**, *68*, 1092-1099.

(59) Pekerar, S.; Lehmann, T.; Méndez, B.; Acevedo, S. *Energy Fuels* **1998**, *13*, 305-308.

(60) Douda, J.; Alvarez, R.; Navarrete Bolaños, J. *Energy Fuels* **2008**, *22*, 2619-2628.

(61) Daaou, M.; Bendedouch, D.; Modarressi, A.; Rogalski, M. *Energy Fuels* **2012**, *26*, 5672-5678.

(62) Daaou, M.; Bendedouch, D.; Bouhadda, Y.; Vernex-Loset, L.; Modaressi, A.; Rogalski, M. *Energy Fuels* **2009**, *23*, 5556-5563.

(63) Bouhadda, Y.; Florian, P.; Bendedouch, D.; Fergoug, T.; Bormann, D. *Fuel* **2010**, *89*, 522-526.

(64) Alemany, L. B.; Verma, M.; Billups, W. E.; Wellington, S. L.; Shammai, M. *Energy Fuels* **2015**, *29* (10), 6317-6329.

(65) Kolodziejski, W.; Klinowski, J. *Chem. Rev.* **2002**, *102* (3), 613-628.

(66) Pomerantz, A. E.; Hammond, M. R.; Morrow, A. L.; Mullins, O. C.; Zare, R. N. *Energy Fuels* **2009**, *23* (3), 1162-1168.

(67) Duer, M. J. In *Solid state NMR spectroscopy: principles and applications*; Duer, M. J., Ed.; Blackwell Science: Oxford, 2002; pp 73–110.

(68) Conte, P.; Berns, A. E. *Anal. Sci.* **2008**, *24*, 1183-1188.

(69) Taylor, R.; Chim, N.; Dybowski, C. *J. Mol. Struct.* **2007**, *830* (1-3), 147-155.

(70) Montina, T.; Hazendonk, P.; Wormald, P.; Iuga, D. *Can. J. Chem.* **2011**, *89*, 1065-1075.

(71) Hazendonk, P.; Wormald, P.; Montina, T. *J. Phys. Chem. A* **2008**, *112*, 6262-6274.

(72) Hazendonk, P.; Harris, R. K.; Ando, S.; Avalle, P. *J. Magn. Reson.* **2003**, *162*, 206-216.

(73) Ando, S.; Harris, R. K.; Reinsberg, S. A. *Magn. Reson. Chem.* **2002**, *40*, 97-106.

(74) Traficante, D. D. Relaxation: An Introduction. *Encyclopedia of Magnetic Resonance* [Online]; John Wiley & Sons, 1996, Posted March 15, 2007. http://dx.doi.org/10.1002/9780470034590.emrstm0452 (accessed Aug 1, 2015).

(75) Moré, J. In *Numerical Analysis SE - 10*; Watson, G. A., Ed.; Lecture Notes in Mathematics; Springer Berlin Heidelberg, 1978; Vol. 630, pp 105–116.

(76) Li, D. D.; Greenfield, M. L. *Energy Fuels* **2011**, *25* (8), 3698-3705.

(77) Bax, A.; Ferretti, J. A.; Nashed, N.; Jerina, D. M. *J. Org. Chem.* **1985**, *50* (17), 3029.

(78) Fechtenkötter, A.; Saalwächter, K.; Harbison, M.; Müllen, K.; Spiess, H. *Angew. Chem. Int. Ed. Engl.* **1999**, *38* (20), 3039-3042.

(79) Fischbach, I.; Pakula, T.; Minkin, P.; Fechtenkötter, A.; Müllen, K.; Spiess, H. W.; Saalwächter, K. *J. Phys. Chem. B* **2002**, *106* (25), 6408-6418.

(80) Smernik, R. J.; Oades, J. M. *Solid State Nucl. Magn. Reson.* **2001**, *20* (1-2), 74-84.

(81) Solum, M. S.; Pugmire, R. J.; Grant, D. M. *Energy Fuels* **1989**, *3*, 187-193.

(82) Pomerantz, A. E.; Hammond, M. R.; Morrow, A. L.; Mullins, O. C.; Zare, R. N. *J. Am. Chem. Soc.* **2008**, *130*, 7216-7217.

(83) Sabbah, H.; Morrow, A. L.; Pomerantz, A. E.; Mullins, O. C.; Tan, X.; Gray, M. R.; Azyat, K.; Tykwinski, R. R.; Zare, R. N. *Energy Fuels* **2010**, *24*, 3589-3594.

(84) Sabbah, H.; Pomerantz, A. E.; Wagner, M.; Müllen, K.; Zare, R. N. *Energy Fuels* **2012**, *26*, 3521-3526.

(85) Sheremata, J. M.; Gray, M. R.; Dettman, H. D.; McCaffrey, W. C. *Energy Fuels* **2004**, *18*, 1377-1384.

(86) Acevedo, S.; Castro, A.; Negrin, J. G.; Fernández, A.; Escobar, G.; Piscitelli, V.; Delolme, F.; Dessalces, G. *Energy Fuels* **2007**, *21* (4), 2165-2175.

(87) Ruiz-Morales, Y.; Mullins, O. C. *Energy Fuels* **2007**, *21* (1), 256-265.

(88) Mullins, O. C. In *Structures and Dynamics of Asphaltenes*; Mullins, O. C., Sheu, E. Y., Eds.; Plenum Pub. Co.: New York, 1998; pp 21–77.

(89) Waldo, G. S.; Mullins, O. C.; Penner-Hahn, J. E.; Cramer, S. P. *Fuel* **1992**, *71* (1), 53-57.